HHS Public Access

Author manuscript

J Bone Miner Res. Author manuscript; available in PMC 2020 March 12.

Published in final edited form as:

J Bone Miner Res. 2020 January ; 35(1): 196–210. doi:10.1002/jbmr.3876.

YAP and TAZ mediate osteocyte perilacunar/canalicular remodeling

Christopher D. Kegelman, B.S.[a,b], **Jennifer C. Coulombe, B.S.**[c], **Kelsey M. Jordan, B.S.**[a,b], **Daniel J. Horan, B.S.**[d], **Ling Qin, Ph.D.**[a], **Alexander G. Robling, Ph.D.**[d], **Virginia. L Ferguson, Ph.D.**[c], **Teresita M. Bellido, Ph.D.**[d], **Joel D. Boerckel, Ph.D.**[a,b,*]

[a.]Department of Orthopaedic Surgery, University of Pennsylvania, Philadelphia, PA, 19104

[b.]Department of Bioengineering, University of Pennsylvania, Philadelphia, PA, 19104

[c.]Department of Mechanical Engineering, University of Colorado, Boulder, CO, 80309

[d.]Department of Anatomy and Cell Biology, Indiana University School of Medicine, Indianapolis, IN, 46202

Abstract

Bone fragility fractures are caused by low bone mass or impaired bone quality. Osteoblast/osteoclast coordination determines bone mass, but the factors that control bone quality are poorly understood. Osteocytes regulate osteoblast and osteoclast activity on bone surfaces but can also directly reorganize the bone matrix to improve bone quality through perilacunar/canalicular remodeling; however, the molecular mechanisms remain unclear. We previously found that deleting the transcriptional regulators Yes-associated protein (YAP) and Transcriptional co-activator with PDZ-motif (TAZ) from osteoblast-lineage cells caused lethality in mice due to skeletal fragility. Here, we tested the hypothesis that YAP and TAZ regulate osteocyte-mediated bone remodeling by conditional ablation of both YAP and TAZ from mouse osteocytes using 8kb-DMP1-Cre. Osteocyte-conditional YAP/TAZ deletion reduced bone mass and dysregulated matrix collagen content and organization, which together decreased bone mechanical properties. Further, YAP/TAZ deletion impaired osteocyte perilacunar/canalicular remodeling by reducing canalicular network density, length, and branching, as well as perilacunar flourochrome-labeled mineral deposition. Consistent with recent studies identifying TGF-β as a key inducer of osteocyte expression of matrix-remodeling enzymes, YAP/TAZ deletion *in vivo* decreased osteocyte expression of matrix proteases MMP13, MMP14, and CTSK. *In vitro*, pharmacologic inhibition of YAP/TAZ transcriptional activity in osteocyte-like cells abrogated TGF-β-induced matrix protease gene expression. Together, these data show that YAP and TAZ control bone matrix accrual, organization, and mechanical properties by regulating osteocyte-mediated bone remodeling. Elucidating the signaling pathways that control perilacunar/canalicular remodeling may enable future therapeutic targeting of bone quality to reverse skeletal fragility.

[*]**To whom correspondence should be addressed:** boerckel@pennmedicine.upenn.edu, Joel D. Boerckel, 376A Stemmler Hall, 3450 Hamilton Walk, University of Pennsylvania, Philadelphia, PA, 19104-6081, Office: 215-246-8186, Fax: 215-573-2133.

DISCLOSURES: The authors have nothing to disclose.

Keywords

osteocytes; genetic animal models; collagen; molecular pathways – remodeling; transcription factors

INTRODUCTION

Skeletal fragility diseases are characterized by decreased bone strength. Bone strength is determined by both the quantity and quality of the bone, both of which are necessary to explain fracture susceptibility[1–3]. Decreased bone mass is a hallmark of osteoporosis, but defects in bone geometry, microarchitecture, porosity, or matrix material properties are significant contributors to bone fragility[4]. Both bone quantity and quality are influenced by bone remodeling, a tightly-coordinated process by which old, damaged bone is resorbed and new, strong bone is deposited. Imbalanced bone remodeling, either by excessive bone resorption or decreased bone formation can impair bone quantity and quality[5,6]. Understanding the mechanisms that control bone remodeling is both scientifically and therapeutically valuable.

The most abundant cell type in bone, osteocytes regulate bone remodeling[7,8]. As terminally differentiated osteoblasts, osteocytes reside within lacunae in the mineralized bone matrix, and extend dendritic processes through an interconnected network of micro-channels called canaliculi that permeate the bone matrix[9–11]. In humans, this lacunar/canalicular network contains an estimated 3.7 trillion dendritic projections and covers more than 215 m^2 of bone surface area[12]. Through this widespread network, osteocyte-derived molecules reach the bone surfaces and regulate bone remodeling by coordinating osteoblast/osteoclast coupled remodeling[13,14]. In addition, osteocytes directly resorb and deposit bone in their surrounding bone matrix via perilacunar/canalicular remodeling[15–17]. However, the molecular mechanisms by which osteocytes control bone remodeling remain poorly understood.

Osteoblast/osteoclast coordinated bone remodeling is regulated in part through the CCN family of matricellular growth factors, cysteine-rich angiogenic inducer-61 (CYR61, CCN1) and connective tissue growth factor (CTGF, CCN2)[18,19]. CYR61 and CTGF have been implicated in activation of osteoblastogenesis[20–23] and inhibition of osteoclastogenesis[24]. Both CYR61 and CTGF are downstream gene targets of the paralogous transcriptional regulators Yes associated protein (YAP) and Transcriptional co-activator with PDZ-binding motif (TAZ)[25,26]. YAP and TAZ are the key effector proteins of the Hippo signaling pathway and regulate important biological functions including organ size determination, tissue regeneration, and cancer[27,28]. Transcriptional complex formation of nuclear YAP and/or TAZ with the transcriptional enhancer activator domain (TEAD) family proteins is required to induce expression of CYR61 and CTGF[25,29].

In addition to paracrine regulation of osteoblast/osteoclast activity, osteocytes directly remodel the bone matrix through perilacunar/canalicular remodeling. Osteocyte perilacunar/canalicular remodeling is regulated by the TGF-β signaling pathway[30]. The TGF-β and YAP/TAZ signaling pathways are known to interact in a variety of cell types including cancer cells, fibroblasts, and epithelial cells[31–34], and the mechanisms by which TGF-β

regulate YAP and TAZ continue to emerge. For example, YAP/TAZ form complexes with the R-SMAD proteins to co-activate TGF-β/SMAD-target gene expression[33,34]. Independent of the R-SMAD proteins, YAP/TAZ interact with additional transcriptional co-factors, such as AP-1 and MRTF, to regulate TGF-β/SMAD-target gene expression[31,32]. Taken together, these observations position YAP and TAZ as potential mediators of TGF-β mediated bone remodeling in osteocytes.

Here, we conditionally ablated both YAP and TAZ from DMP1-expressing cells and evaluated bone remodeling. *In vivo*, we found that osteocyte YAP and TAZ regulate perilacunar/canalicular remodeling as well as coordinate osteoblast/osteoclast activity. *In vitro*, YAP/TAZ inhibition abrogated TGF-β-induced expression of matrix proteases required for osteocyte perilacunar/canalicular remodeling and expression of the matricellular growth factors *Cyr61* and *Ctgf*. Together, these data demonstrate that osteocyte YAP and TAZ control bone matrix accrual, organization, and mechanical properties by regulating osteocyte-mediated bone remodeling.

MATERIALS AND METHODS

Animals

Mice harboring loxP-flanked exon 3 alleles in both YAP and TAZ on a mixed C57BL/6J genetic background were kindly provided by Dr. Eric Olson (University of Texas Southwestern Medical Center). Osteocytes were targeted using Cre-recombination under the control of an 8kb fragment of the dentin matrix protein-1 promoter (8kb-DMP1-Cre)[35]. All mice were fed regular chow (PicoLab Rodent Diet, Cat#: 0007688, LabDiet) *ad libitum* and housed in cages containing 2–5 animals each. Mice were maintained at constant 25°C on a 12-hour light/dark cycle. Mice with homozygous floxed alleles for both YAP and TAZ ($YAP^{fl/fl}$;$TAZ^{fl/fl}$) were mated with double heterozygous conditional knockout mice ($YAP^{fl/+}$;$TAZ^{fl/+}$;DMP1-Cre) to produce eight possible genotypes in each litter, but only the genotypes in Table 1 were compared. Mice were tail or ear clipped after weaning or prior to euthanasia and genotyped by an external service (Transnetyx Inc.). Both male and female mice were evaluated with $YAP^{fl/fl}$;$TAZ^{fl/fl}$ mice serving as littermate wild type (WT) controls. The different analyses were performed in both male and female young mice at either postnatal day 28 (P28) or postnatal day 84 (P84) as indicated. All protocols were approved by the Institutional Animal Care and Use Committees at the University of Notre Dame and the University of Pennsylvania. All animal procedures were performed in adherence to federal guidelines for animal care and conform to the Animal Research: Reporting of In Vivo Experiments (ARRIVE) guidelines.

Microcomputed tomography

Micro-computed tomography (microCT) was performed according to published guidelines[36]. Harvested femurs from P84 mice were stored at −20°C until evaluation. Frozen specimens were thawed and imaged using a vivaCT 80 scanner (Scanco Medical) to determine trabecular and cortical femoral bone architecture prior to mechanical testing. The mid-diaphysis and distal femur were imaged with an X-ray intensity of 114 μA, energy of 70 kVp, integration time of 300 ms, and resolution of 10 μm. Mid-diaphyseal and distal femoral

2D tomograms were manually contoured, stacked and binarized by applying a Gaussian filter (sigma =1, support =1) at a threshold value of 250 mg HA/cm^3. Eight mice were analyzed per group. Investigators were blinded to animal genotype during scan quantification.

Mechanical testing

Following microCT scanning, femurs from P84 mice were tested in three-point bending to failure. Femurs were loaded with the condyles facing down onto the bending fixtures with a support span length of 4.4 mm, which attenuated the effect of femur length on the measured mechanical properties. The upper fixture was aligned with the mid-diaphysis. The femurs were loaded to failure at a rate of 0.5 mm/s using the ElectroForce 3220 Series testing system (TA Instruments). Stiffness, maximum load to failure, work to maximum load and work to failure were quantified using a custom MATLAB script[37]. Eight mice were analyzed per group. Investigators were blinded to animal genotype during data quantification.

Osteocyte lacunae visualization and quantification

Nano-computed tomography (nanoCT) was used to evaluate the morphological characteristics of osteocyte lacunae in the proximal tibia (Xradia Versa XRM-520, Zeiss, Dublin, CA). Tibiae from P84 mice were harvested and removed of all non-osseous tissue. Samples were scanned in 70% EtOH, in custom-made sample holders that oriented the samples vertically on the stage. Tibiae were originally scanned with a 4x objective to determine regions of interest. A 650 μm^3 region of bone was located on the anterior medial aspect of the tibia, 8 mm from the tibiofibular junction (TFJ). Nano-computed tomography images image were collected in the region of interest using a 20× objective with energy settings of 40 V, 3.0 W, using the Air Filter and 3,201 projections. To obtain a constant resolution of 0.6 μm voxel for all the samples, the source and detector distance were varied between 5.8 and 8.5 mm from the sample, and excitation ranged from 6 – 8 seconds contingent on resulting intensity values.

Dragonfly 3.6 (Object Research Systems (ORS) Inc, Montreal, QC) was used for segmentation of bone types and osteocyte lacunae regions. Cortical and trabecular bone were manually segmented. Osteocyte lacunae were identified and segmented in three dimensions using a global Otsu threshold, defined for each sample to most closely match grayscale images[38]. Threshold values were not statistically different between genotypes (31,382 ± 1,080 for YAP^{WT};TAZ^{WT} and 31,032 ± 1,168 for YAP^{cKO};TAZ^{cKO}; $p = 0.83$). Voids that were too small or too large (< 50 μm^3 and > 1,500 μm^3)[39–41] to be an osteocyte lacuna were removed. Osteocyte volume, surface area, and aspect ratio were measured for each osteocyte. Additionally, custom python code based on previous work[39,42,43] was implemented to analyze osteocyte lacunar shape measures, oblateness and stretch. Oblateness and stretch are calculated from the eigenvalues of the shape tensor for each individual osteocyte lacuna. Lacunar oblateness is defined as the “plateness” of a lacuna and ranges from [−1,1], where −1 corresponds to a perfect rod (strongly prolate), and 1 to a perfect plate (strongly oblate)[39].

$$Lc.Ob = 2\left(\frac{\lambda 2 - \lambda 1}{\lambda 3 - \lambda 1}\right) - 1 \quad \text{(Eq. 1)}$$

Similarly, lacunar stretch measures the sphericity of the osteocyte lacunae. Lacunar stretch is evaluated between [0,1], where 0 corresponds to a perfectly spherical, and 1 to an infinitely stretched object[39]

$$Lc.St = \frac{\lambda 3 - \lambda 1}{\lambda 3} \quad \text{(Eq. 2)}$$

Histology, immunohistochemistry, and immunofluorescence

Femurs and tibias from P28 and P84 mice were fixed with 10% neutral buffered formalin for 48 hours at 4°C and decalcified for 4 weeks with 0.25M EDTA (pH 7.4) at 4°C. Paraffin sections (5 μm thickness) were processed for either immunohistochemistry or histology. Primary antibodies were compared to both normal rabbit sera IgG control sections. For immunostaining, anti-CTSK (1:75, ab19027; abcam), anti-MMP13 (1:100, ab39012; abcam), anti-MMP14 (1:100, ab38971; abcam), anti-YAP (1:200, 14074; Cell Signaling), and anti-TAZ (1:200 NB110–58359; Novus Biologicals) primary antibodies were applied overnight. Next, sections were incubated with corresponding biotinylated secondary antibody, avidin-conjugated peroxidase, and diaminobenzidine substrate chromogen system (329ANK-60; Innovex Biosciences), which allowed for immunohistochemical detection of positively stained cells. Hematoxylin and eosin stains (H&E), Tartrate-resistant acid phosphatase (TRAP), Picrosirius Red, and silver nitrate stains were used to stain for osteoblasts, osteoclasts, collagen, and the osteocyte lacunar/canalicular network as previously shown[44,45].

Femurs from P28 mice were fixed with 10% neutral buffered formalin for 48 hours at 4°C, transferred to 30% sucrose in PBS overnight at 4°C, and then embedded in O.C.T. compound (Tissue-Tek). Thin sections (7 μm thickness) were made from undecalcified femurs using cryofilm IIC tape (Section Lab Co. Ltd.) as previously described[46] and processed for immunofluorescence. Taped sections were glued to microscope slides using chitosan adhesive glue, rehydrated and then decalcified with 0.25M EDTA (pH 7.4) for 5 minutes prior to immunofluorescence staining. Terminal deoxynucleotidyl transferase dUTP nick end labeling (TUNEL) assays were then performed using the Click-iT Plus TUNEL Assay kit (C10618; Invitrogen) according to the manufacturer's instructions. Thick sections (20 μm thickness), were processed similarly and stained for F-actin with Alexa Fluor 488-conjugated phalloidin (1:50, Life Technologies) for confocal imaging.

Femurs from P28 mice injected with Calcein (C0875–25G; Sigma-Aldrich) at P21 and Alizarin Complexone (A3882–25G; Sigma Aldrich) at P26 were embedded in methyl-methacrylate and processed for dynamic bone histomorphometry. Using a diamond-embedded wire saw (Delaware Diamond Knives), transverse sections (40 μm) were cut from the midshaft and ground to a final thickness of 20 μm. The slice sections were mounted on slides, and three sections per limb were analyzed.

Imaging and histomorphometric analysis

Histological and immunohistochemical sections were imaged on either a 90i Upright/ Widefield Research Microscope (Nikon Instruments) at the 20× and 40× objectives or an Axio Observer Z1 (Zeiss) at the 20x, 40x, and 63x objectives. Quantification of paraffin immunohistochemistry and histology was performed using ImageJ (NIH) and Osteomeasur™ (OsteoMetrics). To determine the number of positively immunostained cells, 3 fields of view per mouse per antibody were manually scored as either positive or negative and reported as percentage positively stained lacunae per total number of lacunae using ImageJ (NIH). To determine canalicular length, primary canaliculi emanating from each lacuna and extending as a single, unbranched process[30] were traced with ImageJ (NIH). The mean length was taken from at least 5 osteocytes per field within the mid-cortex, with 3 fields per mouse and 6 mice per group[30]. Osteoblast number per bone surface, osteocyte number per bone area, and osteoclast surface per bone surface were quantified using Osteomeasure™ (OsteoMetrics) on H&E and TRAP stained sections in the metaphyseal cancellous bone with 8 mice per group.

The samples tested in three-point bending were stained with Picro-sirius Red to construct a multivariate regression model that included collagen organization and content as a predictor of mechanical behavior. These samples were imaged both under polarized light using an Eclipse ME600 Microscope (Nikon Instruments) at the 20x objective and using second harmonic generated (SHG) microscopy. SHG images were taken on a multiphoton-enabled Fluoview Research Microscope (Olympus) at a fundamental wavelength of 875 nm with the 25x objective on sections oriented in the same direction for all groups. All SHG images were quantified using ImageJ (NIH) and reported as mean pixel intensity within the mid-cortical region relative to WT bone. Mean pixel intensities across four separate regions of interest within each image of the cortex were averaged as technical replicates for a given sample.

Confocal images were acquired using an LSM 710 confocal (Zeiss) with the 63× objective on 20-micron thick sections. 15-micron thick z-stack images were acquired using a step size of 0.5 microns. Three separate regions of interest within the mid-cortex were averaged as technical replicates for a given animal sample. All confocal image stacks were quantified using ImageJ (NIH). Stacks were smoothed by applying a Gaussian filter (sigma = 0.3), then skeletonized using the Skeletonize3D function. The AnalyzeSkeleton2D/3D function was then used to quantify mean branch length, number of branches, and number of junctions[47]. Six YAP^{WT};TAZ^{WT} and four YAP^{cKO};TAZ^{cKO} mice were analyzed.

Immunofluorescence sections of P28 femurs were imaged on an Axio Observer Z1 (Zeiss) at the 20×, 40×, and 63× objectives. To determine the number of positively TUNEL-stained lacunae, 3 fields of view per mouse in the metaphyseal cancellous bone were manually scored as either positive or negative and reported as percent positively stained per total number of lacunae scored in ImageJ (NIH). Dynamic bone histomorphometry parameters were quantified using Osteomeasure™ (OsteoMetrics). The following primary data were collected: total bone surface length (BS); single label perimeter (sL.Pm); double label perimeter (dL.Pm); and double label width (dL.Ith). From primary data, we derived mineralizing surface (MS/BS = [1/2sL.Pm+dL.Pm]/B.Pm ×100; %); mineral apposition rate (MAR = dL.Ith/5 days; μm/day) and bone formation rate (BFR/BS = MAR × MS/BS; μm^3/

μm^2 per day). Six mice were analyzed per group. Investigators were blinded to animal genotype during image acquisition and quantification of all histology, immunohistochemistry, and immunofluorescent images.

Cell culture

IDG-SW3 cells were cultured in α-MEM supplemented with 10% fetal bovine serum, 1% antibiotic/antimycotic (15240062; Gibco) and 1 U/mL INF-γ (PMC4031; Invitrogen) at 33°C. OCY454 cells were cultured in α-minimum essential media (α-MEM) supplemented with 10% fetal bovine serum and 1% antibiotic/antimycotic (Gibco) at 33°C. Prior to treatment, OCY454 cells were differentiated for 12 days at 37°C while IDG-SW3 cells were differentiated for 21 days at 37°C in a-MEM supplemented with 10% fetal bovine serum (100–106; Gemini Bio-Products), 1% antibiotic/antimycotic (15240062; Gibco), 50 μg/ml ascorbic acid (A-4544; Sigma-Aldrich), and 4 mM β-glycerophosphate (G-9422; Sigma-Aldrich) without INF-γ. Prior to treatment on the last day of differentiation, both OCY454 and IDG-SW3 cells were treated with 3 μM verteporfin (SML0534; Sigma-Aldrich) overnight in 1% fetal bovine serum. The next morning, the media was changed and supplemented with 3 μM verteporfin and 5ng/ml TGF-β1 (HZ1011; Humanzyme) for 6 hours before mRNA isolation.

RNA isolation and qPCR

P84 femur samples were dissected and removed of all non-osseous tissue. The ends were cut at the growth plate and marrow flushed before being snap-frozen in liquid nitrogen-cooled isopentane for 1 minute prior to storage at −80°C until processing. Tissues were then homogenized via mortar and pestle and RNA from the sample was collected using Trizol Reagant (15596026; Life Technologies) followed by centrifugation in chloroform. RNA from femur tissue and cell culture experiments were purified using the RNA Easy Kit (74106; Qiagen) and quantified by spectrophotometry using a NanoDrop 2000 (Thermo-Fisher Scientific). Reverse transcriptase polymerase chain reaction (RT-PCR) was performed on 0.5 μg/μl concentration of RNA using the High-Capacity cDNA Reverse Transcription Kit (4368814; Thermo-Fisher Scientific). Quantitative polymerase chain reaction (qPCR) assessed RNA amount using a StepOnePlus™ Real-Time PCR System (Thermo-Fisher Scientific) relative to the internal control of 18S ribosomal RNA (*18S rRNA*). Data are presented using the ΔΔCt method. Six mice per group were used. Specific mouse primer sequences are listed (Supplemental Table 1).

Statistics and regression

Sample sizes were selected *a priori* by power analyses based on effect sizes and population standard deviations taken from published data on $YAP^{fl/fl}$;$TAZ^{fl/fl}$ mice in other tissues[48], assuming a power of 80% and α=0.05. All statistics and regression analyses were performed in GraphPad Prism or using R (Version 3.5.1). Repeated-measures ANOVA with post hoc Tukey's HSD comparison test was performed using R (Version 3.5.1) for osteocyte lacunae quantification. All other comparisons between two groups were made using the two-tailed student's t-test, provided the data were normally distributed according to D'Agostino-Pearson omnibus normality test and homoscedastic according to Bartlett's test in GraphPad Prism. When parametric test assumptions were not met, data were log-transformed, and

residuals were evaluated. If necessary, the non-parametric Mann-Whitney test was used. A p-value < 0.05 was considered significant. Post-hoc power analyses were performed using R (Version 3.5.1) for phenotypic results as indicated (Supplemental Table 2). Data are presented as bars and individual samples with lines corresponding to the mean and standard error of the mean (SEM).

Multivariate regression analyses were performed as described previously[49], using R (Version 3.5.1) with some modifications[37]. Briefly, we used an exhaustive best subsets algorithm to determine the best predictors of maximum load and stiffness from a subset of morphological parameters measured, which included moment of inertia (I) or section modulus (I/c), microCT-measured tissue mineral density (TMD), second harmonic generated (SHG) intensity, and femur length. The best subsets algorithm selects the optimal model using the Akaike's information criterion (AIC), which gives preference to less complex models with fewer explanatory parameters to avoid overfitting the data[50]. The overall "best" multivariate model for each predicted mechanical property was selected with the lowest relative AIC value, indicative of having the least variables with the greatest predictive power.

RESULTS

DMP1-Cre conditionally ablates YAP and TAZ primarily in osteocytes

To determine the roles of YAP and TAZ in osteocyte-mediated bone remodeling, we used Cre-lox to selectively delete YAP and TAZ from 8kb-DMP1-Cre expressing cells[35,51]. We used a breeding strategy that generated YAP/TAZ allele dosage-dependent DMP1-conditional knockouts[37]. All genotypes (Table 1) appeared at expected Mendelian ratios. By early skeletal maturity (P84), YAP/TAZ allele dosage-dependent DMP1-conditional deletion did not significantly alter body mass in either males or females (Supplemental Fig. 1A). YAP/TAZ deletion reduced femoral length at P84 only in double homozygous knockouts, for both sexes (Fig. 1A,B; Supplemental Fig. 1B). A single copy of either gene was sufficient to rescue this defect. Therefore, for further analyses, we selected littermate $YAP^{fl/fl}$;$TAZ^{fl/fl}$ wild type (YAP^{WT};TAZ^{WT}) and $YAP^{fl/fl}$;$TAZ^{fl/fl}$;8kbDMP1-Cre conditional double knockout (YAP^{cKO};TAZ^{cKO}) mice for comparison.

To analyze the specificity of 8kb-DMP1-Cre-mediated YAP/TAZ deletion, we evaluated YAP/TAZ expression in osteocytes, osteoblasts, and growth plate chondrocytes. YAP mRNA expression was significantly reduced by 67% in YAP^{cKO};TAZ^{cKO} femoral bone preparations (Fig. 1C). YAP protein expression was significantly reduced in osteocytes (58% reduction), but not osteoblasts (0% reduction; p = 0.98) (Fig. 1D,E). Similarly, TAZ mRNA expression was significantly reduced by 72% in YAP^{cKO};TAZ^{cKO} femoral bone preparations (Fig. 1F), and TAZ protein expression was significantly reduced in osteocytes (79% reduction), but not osteoblasts (6% reduction; p = 0.12) (Fig. 1G,H). The reduction in YAP^{cKO};TAZ^{cKO} growth plate thickness did not reach statistical significance within the hypertrophic zone (16% reduction; p = 0.26), the proliferating zone (12% reduction; p = 0.39), or total growth plate thickness (13% reduction; p = 0.27; Supplemental Fig. 1C). Further, YAP^{cKO};TAZ^{cKO} growth plate chondrocytes did not show differential expression of YAP or TAZ in either proliferating or hypertrophic zones (Supplemental Fig. 1D–G).

DMP1-conditional YAP/TAZ deletion impaired bone accrual

Dual homozygous YAP/TAZ deletion from DMP1-expressing cells reduced bone accrual and microarchitectural parameters in both the cancellous and cortical compartments of P84 femurs. In metaphyseal cancellous bone, conditional YAP/TAZ deletion significantly reduced bone volume fraction, trabecular number, and thickness and increased trabecular spacing and structural model index (Fig. 2A–F). In mid-diaphyseal femoral cortical bone, conditional YAP/TAZ deletion reduced cortical thickness and bone area without changing medullary area (Fig. 2G–I; Supplemental Fig. 2). Differences in tissue mineral density ($p = 0.24$), periosteal perimeter ($p = 0.15$), and moment of inertia ($p = 0.08$) were not statistically significant (Fig. 2J–L).

To determine if the low bone mass phenotype resulted from decreased bone formation and/or increased bone resorption, we evaluated osteoblast and osteoclast activity. Conditional YAP/TAZ deletion increased osteoclast surface per bone surface (Fig. 3A,B) and decreased osteoblast number per bone surface (Fig. 3C,D) in P84 distal femur metaphyseal cancellous bone. YAP/TAZ deletion decreased bone formation rate, reducing both mineralizing surface percentage and mineral apposition rate at P28 in distal femur metaphyseal cancellous bone (Fig. 3E–H). In the cortical compartment, YAP/TAZ deletion similarly reduced osteoblast number per endosteal bone surface (Supplemental Fig. 3A,B) and decreased bone formation rate by reducing mineral apposition rate without altering mineralizing surface percentage (Supplemental Fig. 3C–F).

Further, YAP/TAZ deletion significantly reduced mRNA expression of YAP/TAZ-TEAD target genes, *Cyr61* and *Ctgf* in femoral bone at P84 (Fig. 3I,J). However, YAP/TAZ deletion did not alter sclerostin (*SOST*), receptor activator of nuclear factor kappa-B ligand (*Rankl*) or osteoprotegerin (*Opg*) transcript expression (Supplemental Fig. 4).

DMP1-conditional YAP/TAZ deletion impaired bone mechanical properties and matrix collagen composition

To determine whether YAP/TAZ deletion impaired functional mechanical properties, we tested P84 femurs in three-point bending to failure (Fig. 4A). Conditional YAP/TAZ deletion did not significantly reduce maximum load to failure (Fig. 4B; $p = 0.07$) but significantly reduced bending stiffness, work to maximum load and work to failure (Fig. 4C–E).

Intrinsic bone material properties are determined, in part, by collagen content and organization[37]. To test whether osteocyte YAP/TAZ regulate the local collagen matrix, we performed polarized light and second harmonic generation (SHG) microscopy (Fig. 4F). YAP/TAZ deletion qualitatively reduced Picrosirius red staining and significantly reduced SHG intensity per bone area, indicative of both collagen content and organization (Fig. 4G). Both cross sectional bone geometry (section modulus and moment of inertia) and collagen matrix content and organization significantly contributed to bone stiffness according to a multivariate best-subsets regression analysis using the Akaike's information criterion (AIC), which selects the model with the lowest number of predictors with the greatest predictive power[37,50]. Neither microCT-measured tissue mineral density nor femur length contributed

to the overall best model according to AIC for stiffness and maximum load to failure (Fig. 4H, Supplemental Fig. 5).

DMP1-conditional YAP/TAZ deletion impaired the osteocyte canalicular network, but not lacunar morphology

We initially hypothesized that the primary function of YAP/TAZ in osteocytes was to regulate expression of genes that control osteocyte-osteoblast and -osteoclast communication, such as secreted factors CYR61 and CTGF. However, the reduced bone mechanical properties and disorganized collagen matrix in mice lacking YAP/TAZ from osteocytes phenocopied matrix metalloproteinase-13 (MMP13) knockout mice, which had defective collagen organization as a result of impaired perilacunar/canalicular remodeling[52]. This led us to ask whether YAP/TAZ deletion from osteocytes impaired perilacunar/canalicular remodeling.

Conditional YAP/TAZ deletion did not significantly alter osteocyte density but increased empty lacunae percentage in cancellous metaphyseal bone (Fig. 5A–C). Accordingly, conditional YAP/TAZ deletion increased the number of TUNEL-positive lacunae, suggesting an increase in osteocyte apoptosis within the cancellous bone compartment (Fig. 5D–E). Conditional YAP/TAZ deletion significantly reduced canalicular density and mean process length, measured in silver nitrate-stained, mid-cortical bone sections (Fig. 5F–H).

As the canalicular system is a three-dimensional network of branched cell processes that physically connect osteocytes to their neighbors[12], we next quantified the 3D canalicular network by laser scanning confocal microscopy of the osteocyte actin cytoskeleton, labeled with phalloidin (Fig. 6A). YAP/TAZ deletion significantly reduced branch length (Fig. 6B,C), number of branches per cell (Fig. 6D), and number of junctions per cell (Fig. 6E).

To determine the effect of YAP/TAZ deletion on osteocyte lacunar morphology, we performed high resolution (0.6 um voxel) X-Ray microscopy (XRM) imaging of both cortical and cancellous bone in the proximal tibia metaphysis (Fig. 6F). YAP/TAZ deletion did not significantly alter lacuna volume (Fig. 6G,H) or shape (Fig. 6I,J), as significant interaction factors were observed between sex, bone compartment, and genotype for all lacunar morphology parameters. Using post-hoc multiple comparisons, no differences in lacunar parameters were observed between genotypes within either a single sex or bone compartment.

DMP1-conditional YAP/TAZ deletion reduced osteocyte-mediated bone matrix remodeling

Perilacunar/canalicular remodeling involves both the deposition and degradation of the bone matrix directly surrounding the osteocytes. Prior studies used ^{3}H-proline pulses and tetracycline labeling to identify osteocyte lacunae as sites of active collagen deposition and mineralization[15,53,54]. Here, we measured collagen I gene expression and flourochrome incorporation in osteocyte lacunae to assess peri-osteocyte matrix deposition. Conditional YAP/TAZ deletion reduced the percentage of Calcein-labeled osteocyte lacunae (Fig. 7A,B) and reduced transcript expression of *Col1a1* (Fig. 7C). However, YAP/TAZ deletion did not alter expression of either osteogenic genes, including alkaline phosphatase (*Alp*), osteocalcin (*Ocn*), and bone sialoprotein (*Bsp*), or osteocyte-marker genes, dentin matrix protein-1

(*Dmp1*) or phosphate-regulating neutral endopeptidase, X-linked (*Phex*) (Supplemental Fig. 6).

In addition to local matrix deposition, osteocytes also locally degrade their extracellular matrix. Many of the matrix metalloproteinases and other enzymes employed by osteoclasts to resorb bone are also expressed by osteocytes and are critical to perilacunar/canalicular remodeling [17,52,55]. Therefore, to test whether YAP/TAZ regulate direct matrix remodeling by osteocytes, we measured mRNA and protein expression of the matrix proteases, cathepsin K (CTSK), matrix metalloproteinase-13 (MMP13), and matrix metalloproteinase-14 (MMP14). Conditional YAP/TAZ deletion reduced the percentage of osteocytes that stained positive for CTSK (Fig. 7D,E), MMP13 (Fig. 7G,H), and MMP14 (Fig. 7J,K) and decreased mRNA expression of *Ctsk* (Fig. 7F), *Mmp13* (Fig. 7I), and *Mmp14* (Fig. 7L) *in vivo*.

YAP/TAZ inhibition abrogated TG-β-induced gene expression in vitro

Though unexplored in osteocytes, YAP and TAZ are known to mediate TGF-β signaling in a variety of other cell types[31–34]. Further, either pharmacologic inhibition or genetic ablation of TGF-β receptors from osteocytes caused defective perilacunar/canalicular remodeling and associated gene expression[30]. Therefore, we next tested whether YAP/TAZ mediate TGF-β signaling, *Cyr61*/*Ctgf* expression, and perilacunar/canalicular remodeling-associated gene expression in osteocytes by treating two osteocyte-like cell lines with combinatorial TGF-β and/or verteporfin (VP) treatment. VP is a small molecule inhibitor that physically blocks the interaction of YAP and TAZ with their transcriptional co-effectors, particularly the TEAD transcription factors, preventing YAP/TAZ-TEAD transcriptional activity[37,56].

We first used mouse osteocyte-derived IDG-SW3 cells, which carry a DMP1 cis-regulatory system driving GFP expression, as a marker of living osteocytes[57,58]. As shown previously, IDG-SW3 cells exhibited robust DMP1-GFP transgene expression after 21 days of *in vitro* osteocytic differentiation (Fig. 8A). Beginning at day 20, cells were treated with vehicle (DMSO) or 3 μM verteporfin (Fig. 8A). At day 21, cells were treated with 5 ng/ml TGF-β or PBS vehicle for 6 hours and gene expression was evaluated by qPCR. Similar experiments were conducted in mouse osteocyte-derived OCY454 cells[59] (Supplemental Fig. 7A).

First, to test whether verteporfin blocked TGF-β-induced YAP/TAZ signaling, we evaluated expression of serpin family E member 1 (*SerpinE1*) and expression of known osteoblast/osteoclast paracrine signaling factors, *Cyr61* and *Ctgf*. Each of these genes are established TGF-β-inducible, YAP/TAZ-TEAD target genes[25,26,60,61]. As expected, TGF-β robustly induced *SerpinE1*, *Cyr61*, and *Ctgf* mRNA expression, which was abrogated by verteporfin treatment (Fig. 8B–D). Next, to test whether YAP/TAZ mediate TGF-β induction of genes associated with perilacunar/canalicular remodeling, we quantified mRNA expression of *Ctsk, Mmp13*, and *Mmp14*. TGF-β significantly induced expression of *Mmp13* and *Mmp14*, but not *Ctsk*, in IDG-SW3 cells, and verteporfin treatment abrogated expression of all three genes (Fig. 8E–G). In OCY454 cells, verteporfin similarly abrogated TGF-β induced expression of *Ctgf, Cyr61* and *SerpinE1* mRNA (Supplemental Fig. 7B–D) as well as *Mmp14* and *Ctsk*, but not *Mmp13* (Supplemental Fig. 7E–G). Finally, we evaluated *Sost*, *Opg*, and *Rankl* expression in both IDG-SW3 and OCY454 cells as potential YAP/TAZ-

regulated mediators of osteocyte-osteoblast/osteoclast signaling. In IDG-SW3 cells, both verteporfin and TGF-β significantly reduced *Sost* transcript expression, while verteporfin abrogated TGF-β-induced *Rankl* and *Opg* expression (Supplemental Fig. 8A–C). In OCY454 cells, verteporfin abrogated TGF-β-induced *Opg* and reduced *Sost* xpression, but did not significantly alter *Rankl* expression (Supplemental Fig. 8D–F). In contrast to IDG-SW3 cells, treatment of OCY454 cells with TGF-β alone significantly reduced *Rankl* transcript expression (Supplemental Fig. 8E).

DISCUSSION

This study identifies new roles of the transcriptional regulators, YAP and TAZ, to enhance our understanding of how osteocyte-mediated bone remodeling contributes to skeletal fragility. Here, we show that YAP and TAZ control bone matrix accrual, organization, and mechanical properties by regulating both perilacunar/canalicular remodeling and osteoblast/osteoclast activity, potentially through TGF-β signaling in osteocytes. Osteocyte-conditional YAP/TAZ deletion reduced bone mass by decreasing osteoblast number and activity and increasing osteoclast activity, but also impaired osteocyte-intrinsic pericellular matrix deposition and degradation, impairing canalicular network connectivity without altering lacunar morphology. *In vitro*, we found that YAP/TAZ activity was required for TGF-β1 induction of matricellular growth factors involved in paracrine signaling from osteocytes to osteoblasts/osteoclasts and matrix proteases necessary for perilacunar/canalicular remodeling. Together, these data identify the transcriptional co-activators YAP and TAZ as key mediators of bone remodeling.

The roles of YAP and TAZ in skeletal-lineage cells are beginning to be clarified. Previously, we reported that dual YAP/TAZ deletion from osteoprogenitor cells and their progeny using Osterix-Cre mimicked severe cases of osteogenesis imperfecta[37]. We identified a combinatorial role for YAP and TAZ in promoting osteoblast number and activity and suppressing osteoclast activity[37]. Similarly, YAP deletion later in the osteoblast lineage, from committed osteoblasts using Osteocalcin-Cre, significantly reduced bone formation, further supporting a role for YAP in promoting osteogenesis *in vivo*[62]. That study did not observe changes in osteoclast activity, potentially due to compensatory effects of TAZ or the Cre line used[62]. We show here that 8kb-DMP1-Creconditional YAP/TAZ deletion from osteocytes also reduced osteoblast number and activity and increased osteoclast activity. Consistent with our data[63], Xiong et al. found that YAP/TAZ deletion using 10kb-DMP1-Cre reduced bone formation and increased osteoclast numbers[64]. The YAP/TAZ-TEAD target, CTGF was previously reported to directly bind to RANKL and OPG to induce osteoclast differentiation *in vitro*[65], but neither the present study nor Xiong et al.[64] observed significant changes in transcript expression of *Sost* or *Opg/Rankl in vivo*. Our *in vitro* experiments in osteocyte-like IDG-SW3 and OCY454 cells did not reveal consistent regulation of *Sost, Opg*, or *Rankl* by YAP/TAZ-TEAD, warranting further mechanistic studies.

Here, we found that YAP/TAZ deletion *in vivo* and inhibition *in vitro* reduced osteocyte expression of the matricellular growth factors, *Cyr61* and *Ctgf*. Both CYR61 and CTGF are induced by TGF-β[60,61] and are transcriptionally regulated directly by the YAP/TAZ-TEAD

complex[25,26]. CYR61 and CTGF are expressed by osteocytes[18] and have been implicated in both osteoblastogenesis[22,23] and osteoclastogenesis[24,66]. During osteoblastogenesis *in vitro*, CYR61 enhances mesenchymal stem cell migration and regulates WNT3A-induced osteogenic differentiation[22]. CTGF also enhances osteoblastogenesis *in vitro*, in part by inhibiting Notch signaling and inducing HES-1 transcription and NFAT transactivation[23]. *In vivo* deletion of CTGF in Osteocalcin-expressing cells led to a mild low bone mass phenotype in male mice without alterations in osteoblast or osteoclast numbers[67]. Similarly, deletion of CYR61 at various stages of the osteoblast lineage (Osterix-Cre, Collagen1(2.3kb)-Cre, and Osteocalcin-Cre) resulted in low bone mass phenotypes of similar severity, suggesting mature osteoblasts/osteocytes are the primary source of CYR61 in bone[19]. Deletion of CYR61 from Osteocalcin-expressing mature osteoblasts also increased osteoclast numbers *in vivo*[19], consistent with the effects of osteocyte-conditional YAP/TAZ deletion here. CYR61 inhibits osteoclastogenesis *in vitro* through a RANKL-independent mechanism[24], while CTGF has been observed to promote osteoclast-precursor fusion through interaction with dendritic cell-specific transmembrane protein (DC-STAMP)[66]. Future studies will be required to dissect the varied mechanisms by which osteocytes direct osteoblast/osteoclast-mediated remodeling, but these data identify a role for YAP/TAZ in osteocyte-mediated promotion of osteoblast activity and suppression of osteoclast activity and implicate a TGF-β–YAP/TAZ-TEAD signaling axis in CYR61 and CTGF expression by osteocytes.

In addition to regulating osteocyte-mediated coordination of osteoblasts and osteoclasts, we found that YAP/TAZ deletion also impaired perilacunar/canalicular remodeling of the bone matrix directly by osteocytes. TGF-β signaling is an osteocyte-intrinsic regulator of perilacunar/canalicular remodeling[30]. Here, we found that DMP1-conditional YAP/TAZ deletion phenocopied the effects of both DMP1-conditional TGF-β receptor deletion and pharmacologic inhibition, which impaired canalicular network length and reduced expression of matrix-degrading enzymes required for perilacunar/canalicular remodeling (i.e. MMP13, MMP14, and CTSK) without altering lacunar morphology[30], as observed here. Confirming the function of these regulated genes, DMP1-conditional YAP/TAZ deletion also partially phenocopied knockout mouse models of these important matrix proteases. First, global knockout of MMP13 in mice osteocyte inhibited perilacunar/canalicular remodeling by reducing collagen organization, flourochrome-labeled mineral deposition around osteocytes, and canalicular network connectivity with similar effect sizes to DMP1-conditional YAP/TAZ deletion[52]. Second, global knockout of MMP14 in mice significantly reduced canalicular network development and maintenance, reducing osteocyte processes density and length[55]. Notably, targeted deletion of MMP14 in skeletal lineage cells using Dermo1-Cre reduced YAP/TAZ activity in osteocytes[68], suggesting a potential feedback loop between matrix protease activity and matrix mechanotransduction. Lastly, global knockout of CTSK in mice impaired bone matrix collagen organization that increased bone fragility in spite of high bone mass and increased osteoclast activity[69]. We therefore pose the working hypothesis that YAP and TAZ act downstream of TGF-β to mediate perilacunar/canalicular remodeling in osteocytes; further investigation will be required to test this *in vivo*.

Perilacunar/canalicular remodeling and osteoblast/osteoclast-mediated remodeling coordinately determine skeletal strength[5,6]. Compromised bone strength caused by defects in bone mass and/or quality results in fragility fracture[4–6]. Bone quantity is primarily regulated by the balance of bone turnover rate while quality includes matrix composition and microarchitectural geometry[4,5]. Both of these factors contribute to the pathogenesis of skeletal fragility diseases such as osteoporosis, Paget's disease, and osteogenesis imperfecta[5]. Here, we found that osteocyte-conditional YAP/TAZ deletion decreased bone mass and altered collagen matrix content and organization, producing moderate defects in bone mechanical behavior. Osteocyte-specific YAP/TAZ knockouts did not exhibit the spontaneous bone fractures prevalent in mice lacking YAP/TAZ in the full osteoblast lineage[37], but their defects correspond with the increased bone fragility described in other models of defective perilacunar/canalicular remodeling[30,52]. Age-related decreases in canalicular network connectivity are associated with microdamage accumulation that contributes to age-associated skeletal fragility[70], further suggesting a contribution of the canalicular network to bone strength.

This study has several limitations. First, small sample sizes (N = 4–8) produced under-powered analyses for some outcome measures. Post-hoc power analyses for indicated perilacunar/canalicular phenotypic results are shown in Supplementary Table 2. Power ranged from 0.74 to 0.99. Thus, not all the studies performed had enough power to compare sex as a variable, though our initial assessment of skeletal phenotype did not show a significant effect of sex. Second, two different age of mice were used (P28 and P84). Both timepoints represent young mice with robust osteocyte canalicular networks avoiding the potentially confounding effects of age-related canalicular network deterioration[70]. However, significant changes in development and bone growth occur in mice between P28 and P84; future studies will characterize the extent of canalicular development during post-natal growth. Third, recent reports suggest that both the 8-kb and 10-kb DMP1 promoter fragments used to drive Cre recombinase expression for conditional ablation in osteocytes can also induce recombination in mature osteoblasts, and other cell types, depending on the sensitivity of the floxed alleles[35,71–73]. Although we observed minimal recombination in osteoblasts and growth plate chondrocytes, the 8-kb DMP1-Cre model used here is not an inducible model, and potential targeting of earlier stage osteogenic cells could still contribute to the developmental changes observed. Fourth, our data suggest that YAP/TAZ act downstream of TGF-β in osteocytes, but continued study will be required to determine whether YAP and TAZ act downstream of TGF-β *in vivo* and to define the transcriptional mechanisms by which YAP and TAZ regulate perilacunar/canalicular remodeling genes. Finally, osteocytes are the key mechanosensing cells in bone[74], and YAP and TAZ are important mediators of mechanotransduction in many cell types[75]; however, the putative roles of YAP and TAZ in osteocyte mechanotransduction are unknown. As mechanical loading also induces perilacunar/canalicular remodeling[76], continued investigation is warranted.

In conclusion, this study identifies the transcriptional co-activators, YAP and TAZ, as regulators of bone quantity and quality that mediate osteocyte regulation of osteoblast/osteoclast activity and perilacunar/canalicular remodeling. Specifically, osteocyte YAP and TAZ are required for the expression of paracrine growth factors that regulate osteoblast/

osteoclast coupled remodeling (i.e., *Cyr61*, *Ctgf*) and the effector enzymes that enable perilacunar/canalicular remodeling. Further elucidation of the mechanisms by which the TGF-β and YAP/TAZ signaling pathways interact to regulate osteocyte function may help guide the development of targeted therapies for the treatment of skeletal fragility diseases.

Supplementary Material

Refer to Web version on PubMed Central for supplementary material.

ACKNOWLEDGEMENTS

$YAP^{fl/fl}$;$TAZ^{fl/fl}$ mice were provided by Dr. Eric Olson (University of Texas Southwestern Medical Center). Theresa Sikorski (University of Notre Dame) provided initial mouse husbandry and maintenance. The authors declare no conflicts of interest. C.D.K. and J.D.B. designed research; C.D.K., J.C.C., K.M.J., A.G.R., V.L.F., T.M.B., and J.D.B. analyzed data; C.D.K., J.C.C., K.M.J., and D.J.H. performed research; J.C.C., D.J.H., A.G.R., L.Q., V.L.F., and T.M.B. contributed new reagents/analytic tools; C.D.K. and J.D.B. wrote the paper; All authors reviewed and approved the paper. C.D.K and J.D.B. take responsibility for integrity of data analysis. This work was supported by the National Institute of Arthritis, Musculoskeletal, and Skin Diseases (NIAMS) of the National Institutes of Health through grants T32 AR007132 (to C.D.K.), P30 AR069619 (to J.D.B.), and R21 AR071559 (to J.D.B., A.G.R., and T.M.B.).

GRANT SUPPORTERS: This work was supported by the National Institute of Arthritis, Musculoskeletal, and Skin Diseases (NIAMS) of the National Institutes of Health through grants T32 AR007132 (to C.D.K.), P30 AR069619 (to J.D.B.), and R21 AR071559 (to J.D.B., A.G.R., and T.M.B.).

REFERENCES

1. Schuit SC., van der Klift M, Weel AEA., et al. Fracture incidence and association with bone mineral density in elderly men and women: the Rotterdam Study. Bone. 2004;34(1):195–202. doi:10.1016/J.BONE.2003.10.001 [PubMed: 14751578]
2. Delmas P, Li Z, Cooper C. Relationship Between Changes in Bone Mineral Density and Fracture Risk Reduction With Antiresorptive Drugs: Some Issues With Meta-Analyses. J Bone Miner Res. 2003;19(2):330–337. doi:10.1359/JBMR.0301228 [PubMed: 14969404]
3. Sarkar S, Mitlak BH, Wong M, Stock JL, Black DM, Harper KD. Relationships Between Bone Mineral Density and Incident Vertebral Fracture Risk with Raloxifene Therapy. J Bone Miner Res. 2002;17(1):1–10. doi:10.1359/jbmr.2002.17.1.1 [PubMed: 11771654]
4. Hernandez CJ, Keaveny TM. A biomechanical perspective on bone quality. Bone. 2006;39(6):1173–1181. doi:10.1016/j.bone.2006.06.001 [PubMed: 16876493]
5. Tranquilli Leali P, Doria C, Zachos A, et al. Bone fragility: current reviews and clinical features. Clin Cases Miner Bone Metab. 2009;6(2):109–113. http://www.ncbi.nlm.nih.gov/pubmed/22461157. Accessed October 9, 2018. [PubMed: 22461157]
6. Recker R, Lappe J, Davies KM, Heaney R. Bone Remodeling Increases Substantially in the Years After Menopause and Remains Increased in Older Osteoporosis Patients. J Bone Miner Res. 2004;19(10):1628–1633. doi:10.1359/JBMR.040710 [PubMed: 15355557]
7. Bellido T Osteocyte-driven bone remodeling. Calcif Tissue Int. 2014;94(1):25–34. doi:10.1007/s00223-013-9774-y [PubMed: 24002178]
8. Prideaux M, Findlay DM, Atkins GJ. Osteocytes: The master cells in bone remodelling. Curr Opin Pharmacol. 2016;28:24–30. doi:10.1016/J.COPH.2016.02.003 [PubMed: 26927500]
9. Franz-Odendaal TA, Hall BK, Witten PE. Buried alive: How osteoblasts become osteocytes. Dev Dyn. 2006;235(1):176–190. doi:10.1002/dvdy.20603 [PubMed: 16258960]
10. Palumbo C, Palazzini S, Zaffe D, Marotti G. Osteocyte Differentiation in the Tibia of Newborn Rabbit: An Ultrastructural Study of the Formation of Cytoplasmic Processes. Cells Tissues Organs. 1990;137(4):350–358. doi:10.1159/000146907
11. Knothe Tate ML, Adamson JR, Tami AE, Bauer TW. The osteocyte. Int J Biochem Cell Biol. 2004;36(1):1–8. doi:10.1016/S1357-2725(03)00241-3 [PubMed: 14592527]

12. Buenzli PR, Sims NA. Quantifying the osteocyte network in the human skeleton. Bone. 2015;75:144–150. doi:10.1016/J.BONE.2015.02.016 [PubMed: 25708054]
13. Hattner R, Epker BN, Frost HM. Suggested sequential mode of control of changes in cell behaviour in adult bone remodelling. Nature. 1965;206(983):489–490. http://www.ncbi.nlm.nih.gov/pubmed/5319106. Accessed October 10, 2018. [PubMed: 5319106]
14. Marotti G, Ferretti M, Muglia MA, Palumbo C, Palazzini S. A quantitative evaluation of osteoblastosteocyte relationships on growing endosteal surface of rabbit tibiae. Bone. 1992;13(5):363–368. http://www.ncbi.nlm.nih.gov/pubmed/1419377. Accessed October 10, 2018. [PubMed: 1419377]
15. Baylink D, Wergedal J Bone formation by osteocytes. Am J Physiol Content. 1971;221(3):669–678. doi:10.1152/ajplegacy.1971.221.3.669
16. Qing H, Bonewald LF. Osteocyte Remodeling of the Perilacunar and Pericanalicular Matrix. Int J Oral Sci. 2009;1(2):59–65. doi:10.4248/ijos.09019 [PubMed: 20687297]
17. Qing H, Ardeshirpour L, Pajevic PD, et al. Demonstration of osteocytic perilacunar/canalicular remodeling in mice during lactation. J Bone Miner Res. 2012;27(5):1018–1029. doi:10.1002/jbmr.1567 [PubMed: 22308018]
18. Kawaki H, Kubota S, Suzuki A, et al. Differential roles of CCN family proteins during osteoblast differentiation: Involvement of Smad and MAPK signaling pathways. Bone. 2011;49(5):975–989. doi:10.1016/J.BONE.2011.06.033 [PubMed: 21763478]
19. Zhao G, Huang B-L, Rigueur D, et al. CYR61/CCN1 Regulates Sclerostin Levels and Bone Maintenance. J Bone Miner Res. 3 2018. doi:10.1002/jbmr.3394
20. Su J-L, Chiou J, Tang C-H, et al. CYR61 regulates BMP-2-dependent osteoblast differentiation through the {alpha}v{beta}3 integrin/integrin-linked kinase/ERK pathway. J Biol Chem. 2010;285(41):31325–31336. doi:10.1074/jbc.M109.087122 [PubMed: 20675382]
21. Chen C-Y, Su C-M, Huang Y-L, Tsai C-H, Fuh L-J, Tang C-H. CCN1 induces oncostatin M production in osteoblasts via integrin-dependent signal pathways. PLoS One. 2014;9(9):e106632. doi:10.1371/journal.pone.0106632
22. Si W, Kang Q, Luu HH, et al. CCN1/Cyr61 is regulated by the canonical Wnt signal and plays an important role in Wnt3A-induced osteoblast differentiation of mesenchymal stem cells. Mol Cell Biol. 2006;26(8):2955–2964. doi:10.1128/MCB.26.8.2955-2964.2006 [PubMed: 16581771]
23. Smerdel-Ramoya A, Zanotti S, Deregowski V, Canalis E. Connective tissue growth factor enhances osteoblastogenesis in vitro. J Biol Chem. 2008;283(33):22690–22699. doi:10.1074/jbc.M710140200 [PubMed: 18583340]
24. Crockett JC, Schütze N, Tosh D, et al. The Matricellular Protein CYR61 Inhibits Osteoclastogenesis by a Mechanism Independent of $\alpha_v\beta_3$ and $\alpha_v\beta_5$. Endocrinology. 2007;148(12):5761–5768. doi:10.1210/en.2007-0473 [PubMed: 17823253]
25. Zhao B, Ye X, Yu J, et al. TEAD mediates YAP-dependent gene induction and growth control. Genes Dev. 2008;22(14):1962–1971. doi:10.1101/GAD.1664408 [PubMed: 18579750]
26. Zhang H, Liu C-Y, Zha Z-Y, et al. TEAD transcription factors mediate the function of TAZ in cell growth and epithelial-mesenchymal transition. J Biol Chem. 2009;284(20):13355–13362. doi:10.1074/jbc.M900843200 [PubMed: 19324877]
27. Yu F-X, Zhao B, Guan K-L. Hippo Pathway in Organ Size Control, Tissue Homeostasis, and Cancer. Cell. 2015;163(4):811–828. doi:10.1016/j.cell.2015.10.044 [PubMed: 26544935]
28. Mo J-S, Park HW, Guan K-L. The Hippo signaling pathway in stem cell biology and cancer. EMBO Rep. 2014;15(6):642–656. doi:10.15252/embr.201438638 [PubMed: 24825474]
29. Zhang H, Pasolli HA, Fuchs E. Yes-associated protein (YAP) transcriptional coactivator functions in balancing growth and differentiation in skin. Proc Natl Acad Sci U S A. 2011;108(6):2270–2275. doi:10.1073/pnas.1019603108 [PubMed: 21262812]
30. Dole NS, Mazur CM, Acevedo C, et al. Osteocyte-Intrinsic TGF-β Signaling Regulates Bone Quality through Perilacunar/Canalicular Remodeling. Cell Rep. 2017;21(9):2585–2596. doi:10.1016/j.celrep.2017.10.115 [PubMed: 29186693]
31. Qin Z, Xia W, Fisher GJ, Voorhees JJ, Quan T. YAP/TAZ regulates TGF-β/Smad3 signaling by induction of Smad7 via AP-1 in human skin dermal fibroblasts. Cell Commun Signal. 2018;16(1):18. doi:10.1186/s12964-018-0232-3 [PubMed: 29695252]

32. Miranda MZ, Bialik JF, Speight P, et al. TGF-β1 regulates the expression and transcriptional activity of TAZ protein via a Smad3-independent, myocardin-related transcription factor-mediated mechanism. J Biol Chem. 2017;292(36):14902–14920. doi:10.1074/jbc.M117.780502 [PubMed: 28739802]
33. Varelas X, Sakuma R, Samavarchi-Tehrani P, et al. TAZ controls Smad nucleocytoplasmic shuttling and regulates human embryonic stem-cell self-renewal. Nat Cell Biol. 2008;10(7):837–848. doi:10.1038/ncb1748 [PubMed: 18568018]
34. Varelas X, Samavarchi-Tehrani P, Narimatsu M, et al. The Crumbs complex couples cell density sensing to Hippo-dependent control of the TGF-β-SMAD pathway. Dev Cell. 2010;19(6):831–844. doi:10.1016/j.devcel.2010.11.012 [PubMed: 21145499]
35. Bivi N, Condon KW, Allen MR, et al. Cell autonomous requirement of connexin 43 for osteocyte survival: Consequences for endocortical resorption and periosteal bone formation. J Bone Miner Res. 2012;27(2):374–389. doi:10.1002/jbmr.548 [PubMed: 22028311]
36. Bouxsein ML, Boyd SK, Christiansen BA, Guldberg RE, Jepsen KJ, Müller R. Guidelines for assessment of bone microstructure in rodents using micro-computed tomography. J Bone Miner Res. 2010;25(7):1468–1486. doi:10.1002/jbmr.141 [PubMed: 20533309]
37. Kegelman CD, Mason DE, Dawahare JH, et al. Skeletal cell YAP and TAZ combinatorially promote bone development. FASEB J. 2018;32(5):2706–2721. doi:10.1096/fj.201700872R [PubMed: 29401582]
38. Otsu N A threshold selection method from gray-level histograms. IEEE Trans Syst Man Cybern. 1979;9(1):62–66.
39. Mader KS, Schneider P, Müller R, Stampanoni M. A quantitative framework for the 3D characterization of the osteocyte lacunar system. Bone. 2013;57(1):142–154. doi:10.1016/J.BONE.2013.06.026 [PubMed: 23871748]
40. Hemmatian H, Laurent MR, Bakker AD, Vanderschueren D, Klein-Nulend J, van Lenthe GH. Agerelated changes in female mouse cortical bone microporosity. Bone. 2018;113:1–8. doi:10.1016/J.BONE.2018.05.003 [PubMed: 29738854]
41. Tiede-Lewis LM, Xie Y, Hulbert MA, et al. Degeneration of the osteocyte network in the C57BL/6 mouse model of aging. Aging (Albany NY). 2017;9(10):2190–2208. doi:10.18632/aging.101308 [PubMed: 29074822]
42. Heveran CM, Rauff A, King KB, Carpenter RD, Ferguson VL. A new open-source tool for measuring 3D osteocyte lacunar geometries from confocal laser scanning microscopy reveals age-related changes to lacunar size and shape in cortical mouse bone. Bone. 2018;110:115–127. doi:10.1016/j.bone.2018.01.018 [PubMed: 29374550]
43. McCreadie BR, Hollister SJ, Schaffler MB, Goldstein SA. Osteocyte lacuna size and shape in women with and without osteoporotic fracture. J Biomech. 2004;37(4):563–572. doi:10.1016/S0021-9290(03)00287-2 [PubMed: 14996569]
44. Ploton D, Menager M, Jeannesson P, Himber G, Pigeon F, Adnet JJ. Improvement in the staining and in the visualization of the argyrophilic proteins of the nucleolar organizer region at the optical level. Histochem J. 1986;18(1):5–14. http://www.ncbi.nlm.nih.gov/pubmed/2423479. Accessed August 9, 2018. [PubMed: 2423479]
45. Jáuregui EJ, Akil O, Acevedo C, et al. Parallel mechanisms suppress cochlear bone remodeling to protect hearing. Bone. 2016;89:7–15. doi:10.1016/j.bone.2016.04.010 [PubMed: 27085457]
46. Dyment NA, Jiang X, Chen L, et al. High-Throughput, Multi-Image Cryohistology of Mineralized Tissues. J Vis Exp. 2016;(115):e54468-e54468. doi:10.3791/54468
47. Arganda-Carreras I, Fernández-González R, Muñoz-Barrutia A, Ortiz-De-Solorzano C. 3D reconstruction of histological sections: Application to mammary gland tissue. Microsc Res Tech. 2010;73(11):1019–1029. doi:10.1002/jemt.20829 [PubMed: 20232465]
48. Xin M, Kim Y, Sutherland LB, et al. Hippo pathway effector Yap promotes cardiac regeneration. Proc Natl Acad Sci U S A. 2013;110(34):13839–13844. doi:10.1073/pnas.1313192110 [PubMed: 23918388]
49. Schneider P, Voide R, Stampanoni M, Donahue LR, Müller R. The importance of the intracortical canal network for murine bone mechanics. Bone. 2013;53(1):120–128. doi:10.1016/j.bone.2012.11.024 [PubMed: 23219945]

50. Akaike H A new look at the statistical model identification. IEEE Trans Automat Contr. 1974;19(6):716–723. doi:10.1109/TAC.1974.1100705
51. Delgado-Calle J, Tu X, Pacheco-Costa R, et al. Control of Bone Anabolism in Response to Mechanical Loading and PTH by Distinct Mechanisms Downstream of the PTH Receptor. J Bone Miner Res. 2017;32(3):522–535. doi:10.1002/jbmr.3011 [PubMed: 27704638]
52. Tang SY, Herber R-P, Ho SP, Alliston T. Matrix metalloproteinase-13 is required for osteocytic perilacunar remodeling and maintains bone fracture resistance. J Bone Miner Res. 2012;27(9):1936–1950. doi:10.1002/jbmr.1646 [PubMed: 22549931]
53. Zambonin Zallone AZ, Teti A, Nico B, Primavera M V. Osteoplastic activity of mature osteocytes evaluated by H-proline incorporation. Basic Appl Histochem. 1982;26(1):65–67. http://www.ncbi.nlm.nih.gov/pubmed/7082267. Accessed March 24, 2019. [PubMed: 7082267]
54. Zambonin Zallone A, Teti A, Primavera MV, Pace G. Mature osteocytes behaviour in a repletion period: the occurrence of osteoplastic activity. Basic Appl Histochem. 1983;27(3):191–204. http://www.ncbi.nlm.nih.gov/pubmed/6196018. Accessed March 24, 2019. [PubMed: 6196018]
55. Holmbeck K, Bianco P, Pidoux I, et al. The metalloproteinase MT1-MMP is required for normal development and maintenance of osteocyte processes in bone. J Cell Sci. 2005;118(1):147–156. doi:10.1242/jcs.01581 [PubMed: 15601659]
56. Liu-Chittenden Y, Huang B, Shim JS, et al. Genetic and pharmacological disruption of the TEAD-YAP complex suppresses the oncogenic activity of YAP. Genes Dev. 2012;26(12):1300–1305. doi:10.1101/gad.192856.112 [PubMed: 22677547]
57. Kalajzic I, Braut A, Guo D, et al. Dentin matrix protein 1 expression during osteoblastic differentiation, generation of an osteocyte GFP-transgene. Bone. 2004;35(1):74–82. doi:10.1016/J.BONE.2004.03.006 [PubMed: 15207743]
58. Woo SM, Rosser J, Dusevich V, Kalajzic I, Bonewald LF. Cell line IDG-SW3 replicates osteoblast-to-late-osteocyte differentiation in vitro and accelerates bone formation in vivo. J Bone Miner Res. 2011;26(11):2634–2646. doi:10.1002/jbmr.465 [PubMed: 21735478]
59. Spatz JM, Wein MN, Gooi JH, et al. The Wnt Inhibitor Sclerostin Is Up-regulated by Mechanical Unloading in Osteocytes in Vitro. J Biol Chem. 2015;290(27):16744–16758. doi:10.1074/jbc.M114.628313 [PubMed: 25953900]
60. Bartholin L, Wessner LL, Chirgwin JM, Guise TA. The human Cyr61 gene is a transcriptional target of transforming growth factor beta in cancer cells. Cancer Lett. 2007;246(1–2):230–236. doi:10.1016/J.CANLET.2006.02.019 [PubMed: 16616811]
61. Grotendorst GR. Connective tissue growth factor: a mediator of TGF-beta action on fibroblasts. Cytokine Growth Factor Rev. 1997;8(3):171–179. http://www.ncbi.nlm.nih.gov/pubmed/9462483. Accessed March 10, 2019. [PubMed: 9462483]
62. Pan J-X, Xiong L, Zhao K, et al. YAP promotes osteogenesis and suppresses adipogenic differentiation by regulating β-catenin signaling. Bone Res. 2018;6(1):18. doi:10.1038/s41413-018-0018-7 [PubMed: 29872550]
63. Kegelman CD, Mason DE, Dawahare JH, et al. Skeletal cell YAP and TAZ redundantly promote bone development by regulation of collagen I expression and organization. bioRxiv. 5 2017:143982. doi:10.1101/143982
64. Xiong J, Almeida M, O'Brien CA. The YAP/TAZ transcriptional co-activators have opposing effects at different stages of osteoblast differentiation. Bone. 2018;112:1–9. doi:10.1016/J.BONE.2018.04.001 [PubMed: 29626544]
65. Aoyama E, Kubota S, Khattab HM, Nishida T, Takigawa M. CCN2 enhances RANKL-induced osteoclast differentiation via direct binding to RANK and OPG. Bone. 2015;73:242–248. doi:10.1016/j.bone.2014.12.058 [PubMed: 25554597]
66. Nishida T, Emura K, Kubota S, Lyons KM, Takigawa M. CCN family 2/connective tissue growth factor (CCN2/CTGF) promotes osteoclastogenesis via induction of and interaction with dendritic cell-specific transmembrane protein (DC-STAMP). J Bone Miner Res. 2011;26(2):351–363. doi:10.1002/jbmr.222 [PubMed: 20721934]
67. Canalis E, Zanotti S, Beamer WG, Economides AN, Smerdel-Ramoya A. Connective Tissue Growth Factor Is Required for Skeletal Development and Postnatal Skeletal Homeostasis in Male Mice. Endocrinology. 2010;151(8):3490–3501. doi:10.1210/en.2010-0145 [PubMed: 20534727]

68. Tang Y, Rowe RG, Botvinick EL, et al. MT1-MMP-Dependent Control of Skeletal Stem Cell Commitment via a β1-Integrin/YAP/TAZ Signaling Axis. Dev Cell. 2013;25(4):402–416. doi:10.1016/j.devcel.2013.04.011 [PubMed: 23685250]
69. Li CY, Jepsen KJ, Majeska RJ, et al. Mice Lacking Cathepsin K Maintain Bone Remodeling but Develop Bone Fragility Despite High Bone Mass. J Bone Miner Res. 2006;21(6):865–875. doi:10.1359/jbmr.060313 [PubMed: 16753017]
70. Vashishth D, Verborgt O, Divine G, Schaffler MB, Fyhrie DP. Decline in osteocyte lacunar density in human cortical bone is associated with accumulation of microcracks with age. Bone. 2000;26(4):375–380. doi:10.1016/S8756-3282(00)00236-2 [PubMed: 10719281]
71. O'Brien CA, Plotkin LI, Galli C, et al. Control of Bone Mass and Remodeling by PTH Receptor Signaling in Osteocytes. Jin D-Y, ed. PLoS One. 2008;3(8):e2942. doi:10.1371/journal.pone.0002942
72. Xiong J, Piemontese M, Onal M, et al. Osteocytes, not Osteoblasts or Lining Cells, are the Main Source of the RANKL Required for Osteoclast Formation in Remodeling Bone. Heymann D, ed. PLoS One. 2015;10(9):e0138189. doi:10.1371/journal.pone.0138189
73. Rhee Y, Allen MR, Condon K, et al. PTH receptor signaling in osteocytes governs periosteal bone formation and intracortical remodeling. J Bone Miner Res. 2011;26(5):1035–1046. doi:10.1002/jbmr.304 [PubMed: 21140374]
74. Bonewald LF. Mechanosensation and Transduction in Osteocytes. Bonekey Osteovision. 2006;3(10):7–15. doi:10.1138/20060233 [PubMed: 17415409]
75. Dupont S, Morsut L, Aragona M, et al. Role of YAP/TAZ in mechanotransduction. Nature. 2011;474(7350):179–183. doi:10.1038/nature10137 [PubMed: 21654799]
76. Gardinier JD, Al-Omaishi S, Morris MD, Kohn DH. PTH signaling mediates perilacunar remodeling during exercise. Matrix Biol. 2016;52–54:162–175. doi:10.1016/J.MATBIO.2016.02.010

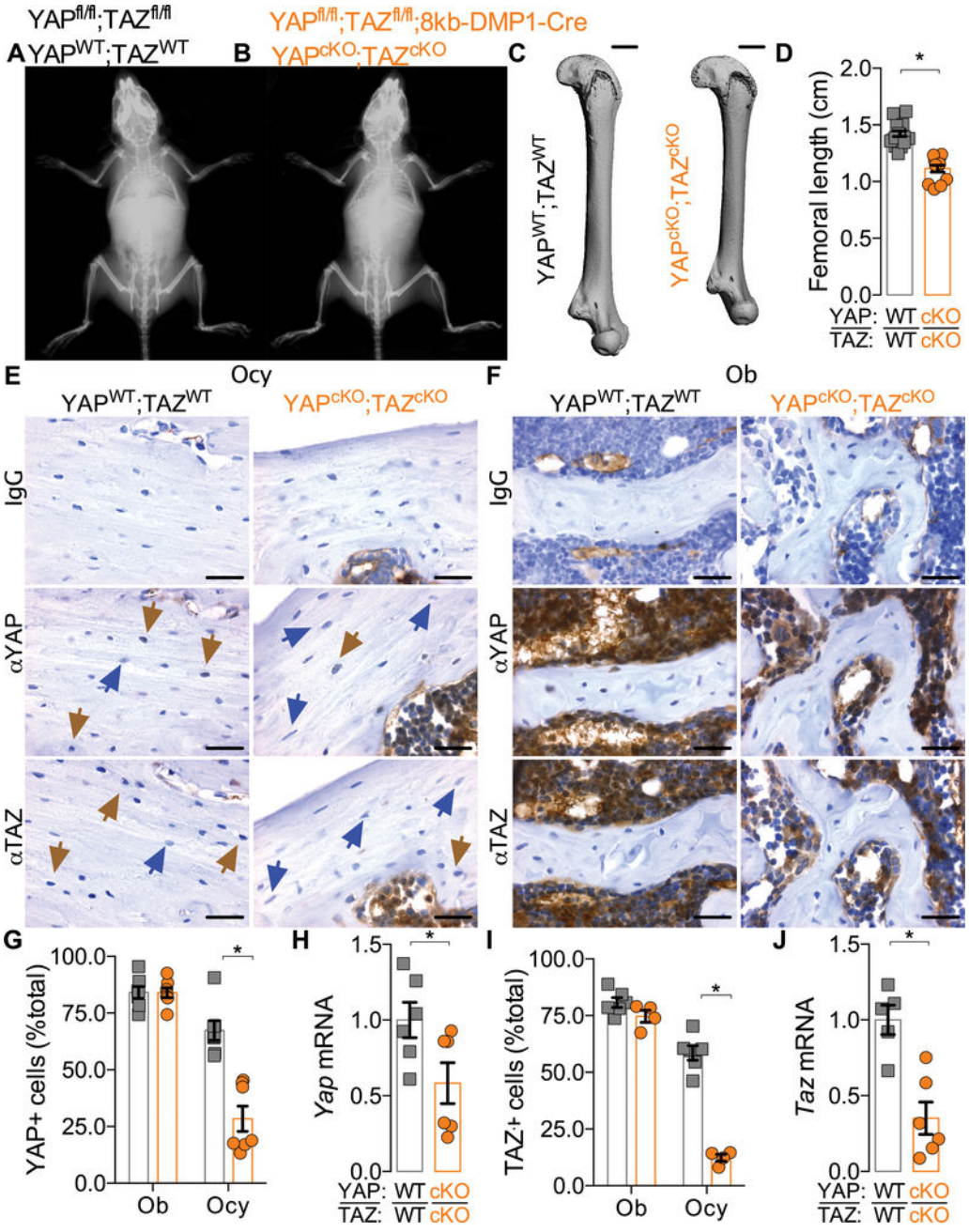

Figure 1. 8kb-DMP1-Cre selectively ablated YAP/TAZ expression from osteocytes.

A) Representative radiographs for P84 wild type ($YAP^{WT};TAZ^{WT}$) and **B)** conditional double knockout ($YAP^{cKO};TAZ^{cKO}$) mice. **C)** P84 femur microCT reconstructions and **D)** quantification of femoral lengths. **E-J)** Recombination efficiency and specificity was assessed by measurement of YAP and TAZ protein and mRNA expression. **E)** Representative micrographs of osteocyte (Ocy) immunostaining for IgG control, YAP, and TAZ in $YAP^{WT};TAZ^{WT}$ and $YAP^{cKO};TAZ^{cKO}$ femurs at P28. **F)** Representative micrographs of osteoblast (Ob) immunostaining for IgG control, YAP, and TAZ in $YAP^{WT};TAZ^{WT}$ and $YAP^{cKO};TAZ^{cKO}$ femurs at P28. **G)** YAP protein expression in

osteocytes (Ocy) and osteoblasts (Ob) from femoral sections at P28. **H)** *Yap* mRNA expression, relative to *18S rRNA*, from femoral bone preparations at P84. **I)** TAZ protein expression in osteocytes (Ocy) and osteoblasts (Ob) from femoral sections at P28. **J)** *Taz* mRNA expression, relative to *18S rRNA*, from femoral bone preparations at P84. Data are presented with individual samples in scatterplots and bars corresponding to the mean and standard error of the mean (SEM). N = 5–6 per group for qPCR and N = 4–6 per group for IHC. Brown arrows indicate positive osteocytes. Blue arrows indicate negative osteocytes. Scale bars equal 1 mm in microCT reconstructions and 30 μm in all images.

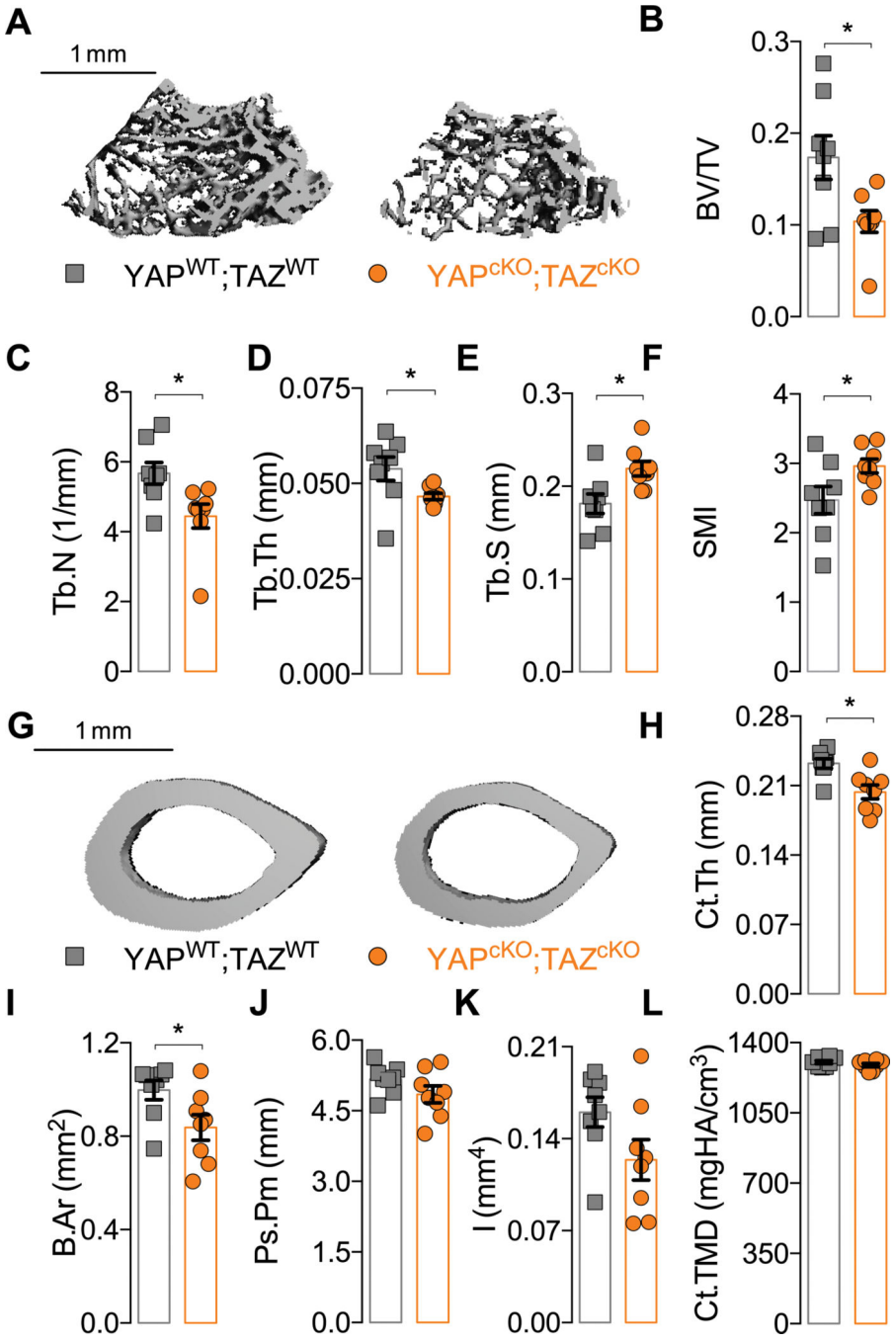

Figure 2. YAP/TAZ ablation from DMP1-expressing cells altered bone microarchitecture.

A) Representative microCT reconstructions of distal metaphysis of P84 femurs. Quantification of cancellous bone microarchitecture: (B) bone volume fraction (BV/TV), (C) trabecular thickness (Tb.Th), (D) number (Tb.N), (E) spacing (Tb.Sp), and (F) structural model index (SMI). G) Representative microCT reconstructions of mid-diaphysis cortical microarchitecture in P84 femurs. Quantification of cortical microarchitectural properties: (H) cortical thickness (Ct.Th), (I) bone area (B.Ar), (J) periosteal perimeter (Ps.Pm), (K) moment of inertia in the direction of bending (I), and (L) cortical tissue mineral density

(Ct.TMD). Data are presented with individual samples in scatterplots and bars corresponding to the mean and standard error of the mean (SEM). Sample sizes, N = 8. Scale bars indicate 1 mm for microCT reconstructions.

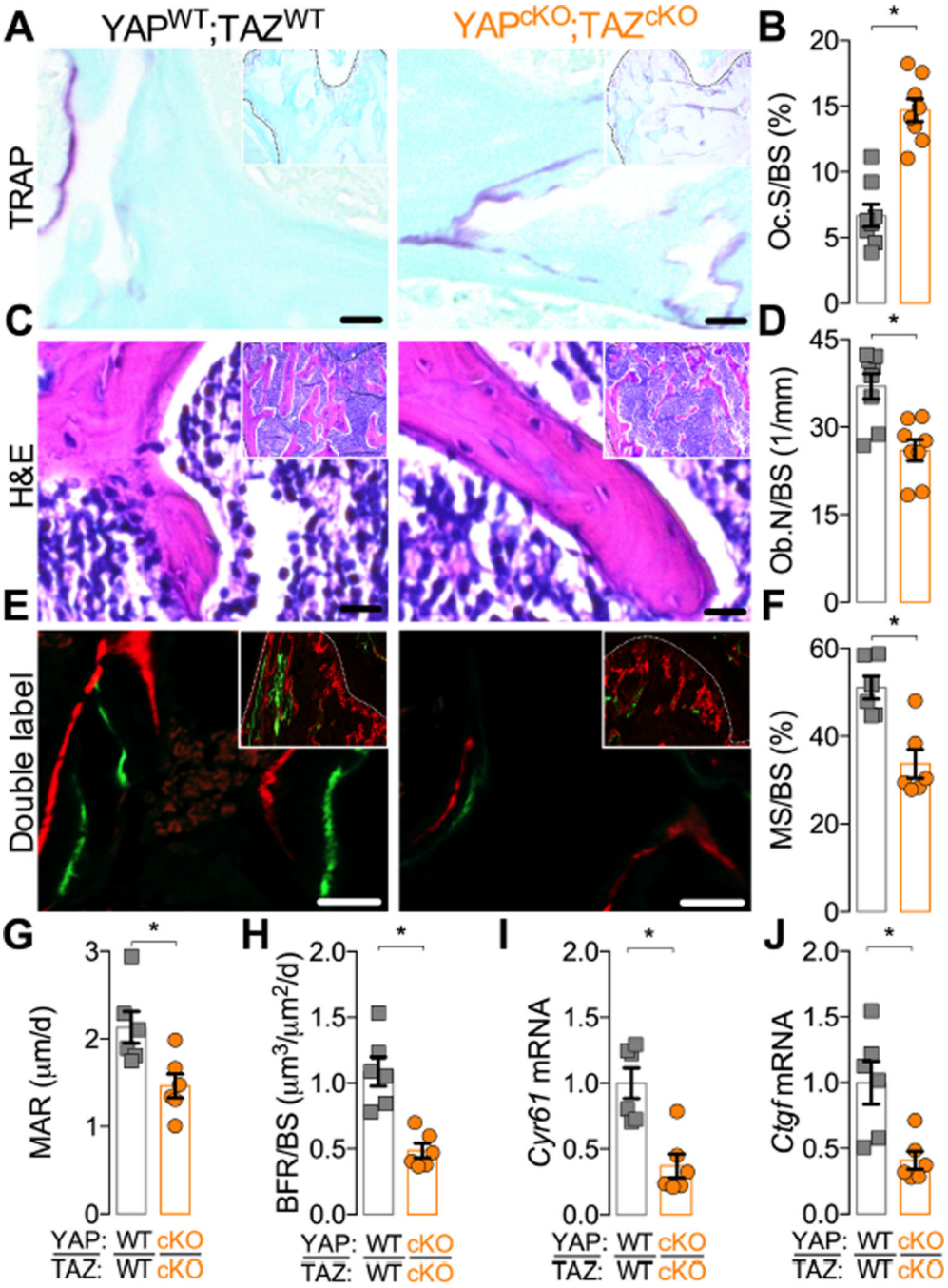

Figure 3. YAP/TAZ ablation from DMP1-expressing cells increased osteoclast activity and decreased osteoblast activity.

A) Representative high magnification micrographs with insets of low magnification micrographs of P84 cancellous metaphyseal bone (outlined in black) stained by TRAP. **B)** Quantification of osteoclast surface per bone surface (Oc.S/BS). **C)** Representative high magnification micrographs with insets of low magnification micrographs of P84 cancellous metaphyseal bone (outlined in black) stained by H+E. **D)** Quantification of osteoblast number per bone surface (Ob.N/BS). **E)** Representative high magnification micrographs

with insets of low magnification micrographs of double flourochrome labeled P28 cancellous metaphyseal bone (outlined in white). **F-H)** Quantification of **(F)** mineralizing surface percentage (MS/BS), **(G)** mineral apposition rate (MAR) and **(H)** bone formation rate (BFR/BS). **I-J)** Femoral bone preparations from P84 mice were harvested to quantify mRNA expression. Expression levels, normalized to *18S rRNA*, were evaluated for **(I)** cysteine-rich angiogenic inducer 61 (*Cyr61*) and **(J)** connective tissue growth factor (*Ctgf*). Data are presented with individual samples in scatterplots and bars corresponding to the mean and standard error of the mean (SEM). Sample sizes N = 6–8. Scale bars indicate 15 μm in all images.

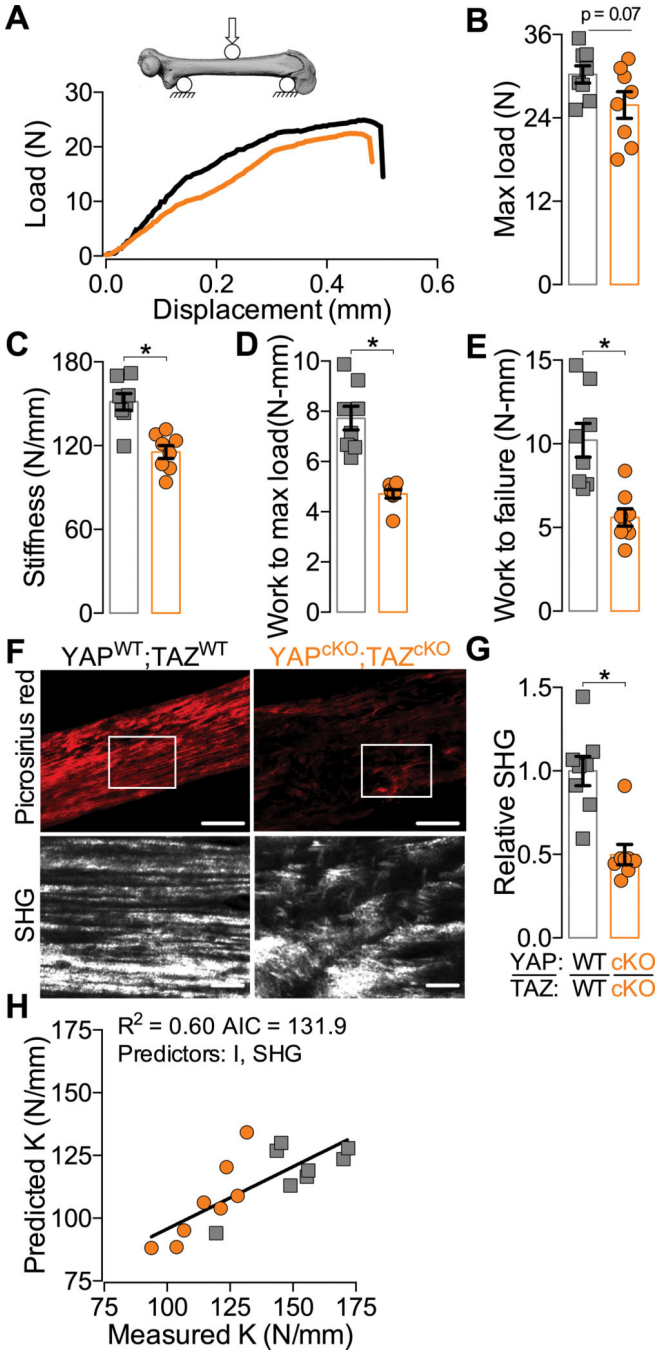

Figure 4. YAP/TAZ ablation from DMP1-expressing cells impaired bone mechanical behavior by altering bone geometry and matrix collagen.

A) P84 femurs were tested in three-point bending to failure. **B-E)** Quantification of **(B)** maximum load to failure, **(C)** bending stiffness, **(D)** work to max load, and **(E)** work to failure. **F)** Representative micrographs of polarized light microscopy and second harmonic generated (SHG) images of cortical bone from the P84 femurs tested in three-point bending. **G-H)** Quantification of **(G)** SHG intensity normalized to wild type. **H)** Best-subset multivariate regression model predicting experimental bending stiffness (K) using moment

of inertia and SHG intensity as predictors. Data are presented with individual samples in scatterplots and bars corresponding to the mean and standard error of the mean (SEM). Sample sizes, N = 8 per group. Scale bars equal 100 and 25 μm in the Picrosirius red and SHG, respectively.

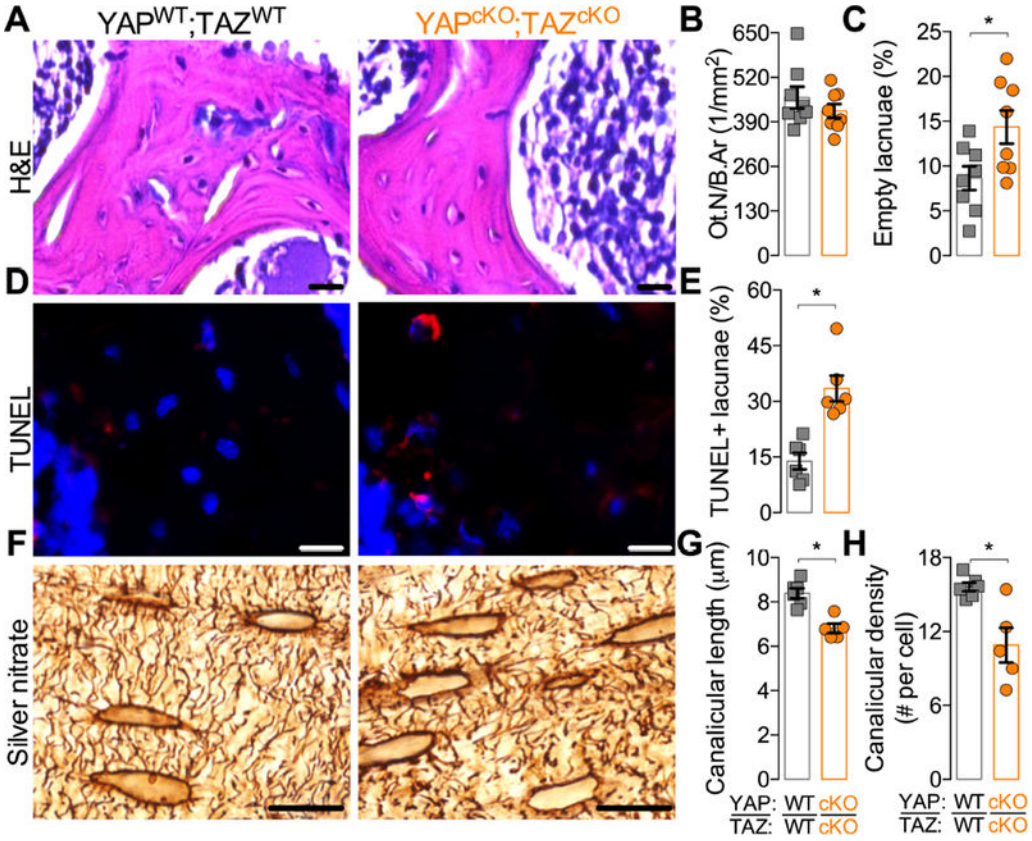

Figure 5. YAP/TAZ ablation from DMP1-expressing cells increased osteocyte apoptosis and reduced canalicular number and length in 2D.

A) Representative micrographs of P84 cancellous metaphyseal bone stained by H+E. **B-C)** Quantification of **(B)** osteocyte number per bone area (Ot.N/B.Ar), and **(C)** percentage of empty lacunae. **D)** Representative immunofluorescence micrographs of P28 cancellous metaphyseal bone stained with TUNEL positive cells (red) and DAPI (blue). **E)** Quantification of the percentage of TUNEL positive lacunae. **F)** Representative micrographs of P84 mid-cortical bone silver stained for the osteocyte canalicular network. **G-H)** Quantification of **(G)** canalicular density per cell and **(H)** average canalicular length. Data are presented with individual samples in scatterplots and bars corresponding to the mean and standard error of the mean (SEM). Sample sizes, N = 6–8 per group. Scale bars equal 15 μm all images.

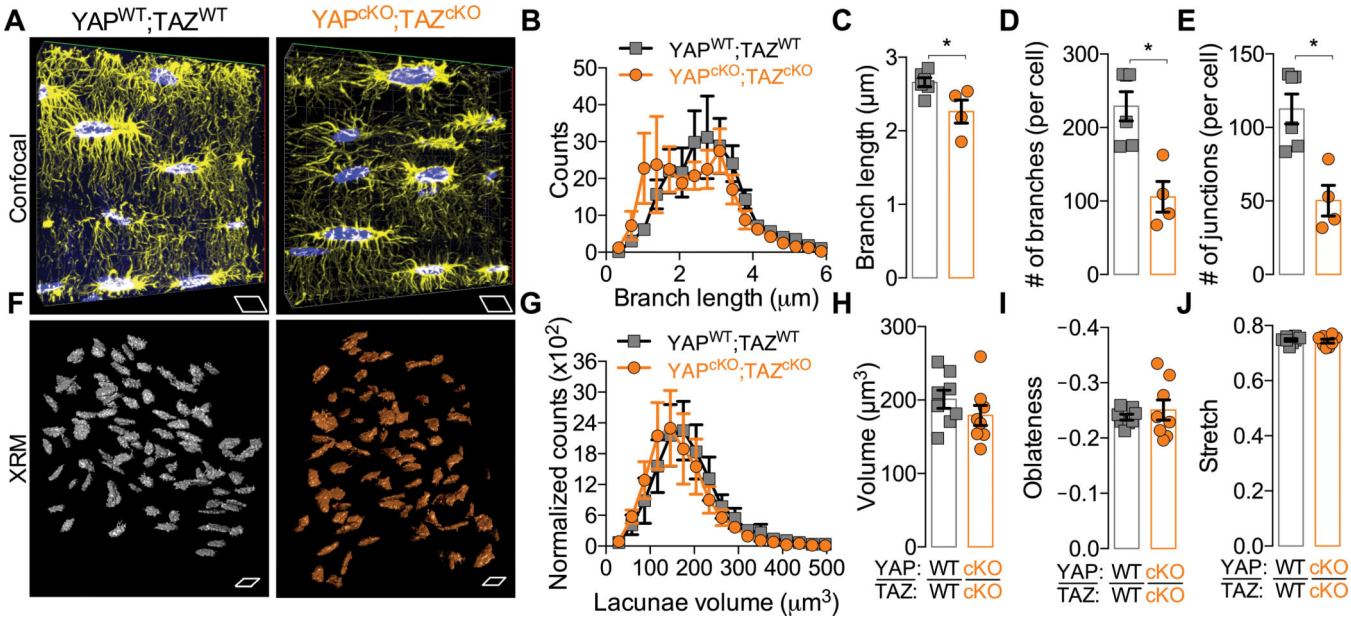

Figure 6. YAP/TAZ ablation from DMP1-expressing cells reduced canalicular network length and branching, but not lacunar morphology in 3D.

A) Representative 15-micron thick confocal reconstructions of phalloidin-stained osteocyte F-actin cytoskeletons in cortical bone at P28. **B)** Average distributions of branch length. **C-E)** Quantification of **(C)** average branch length, **(D)** number of branches, and **(E)** number of junctions. **F)** Representative lacunar morphologies in 3D in cancellous bone from P84 tibiae using X-ray microscopy (XRM). **G)** Average distributions of lacunar volume. **H-J)** Quantification of **(H)** average lacuna volume, **(I)** oblateness, and **(J)** stretch. Data are presented with individual samples in scatterplots and bars corresponding to the mean and standard error of the mean (SEM). Sample sizes, N = 4–6 for confocal network analysis and N = 8 for XRM. Each side of scale parallelograms equal 10 μm for both confocal and XRM.

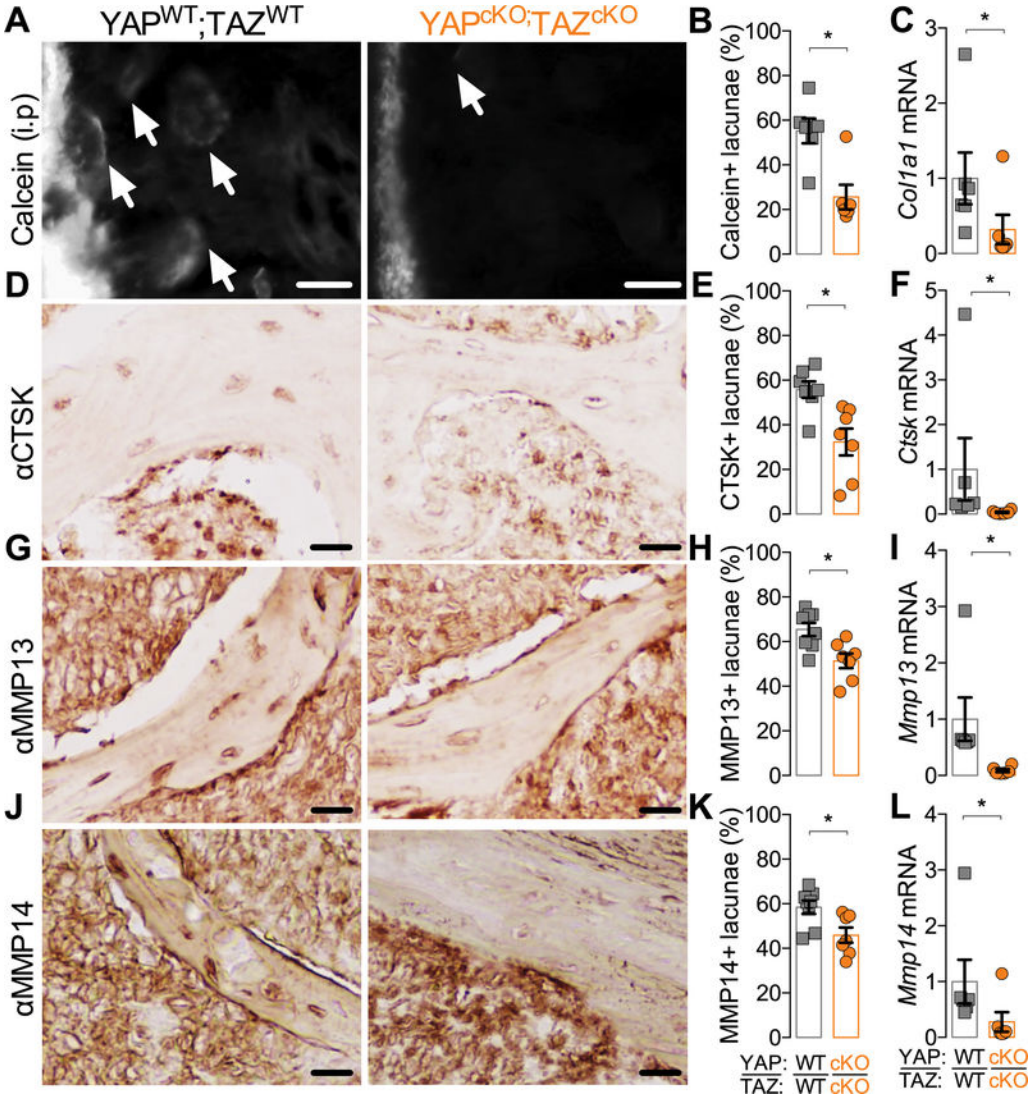

Figure 7. YAP/TAZ ablation from DMP1-expressing cells reduced osteocyte-mediated bone remodeling.

A) Representative double fluorochrome-labeled osteocytes (white) in cortical bone from P28 femurs (Calcein label injected at P21). **B-C)** Quantification of **(B)** Calcein labeled lacunae and **(C)** relative transcript expression for collagen1a1 (*Col1a1*) in P84 femoral bone preparations. **D)** Representative micrographs of cancellous metaphyseal bone from P84 femurs immunostained for cathepsin K (CTSK). **E-F)** Quantification of **(E)** CTSK immunostained lacunae and **(F)** relative transcript expression for *Ctsk* in P84 femoral bone preparations. **G)** Representative micrographs of cancellous metaphyseal bone from P84 femurs immunostained for matrix metalloproteinase 13 (MMP13). **E-F)** Quantification of **(E)** MMP13 immunostained lacunae and **(F)** relative transcript expression for *Mmp13* in P84 femoral bone preparations. **J)** Representative micrographs of cancellous metaphyseal bone from P84 femurs immunostained for matrix metalloproteinase 14 (MMP14). **K-L)** Quantification of **(K)** *MMP14* immunostained lacunae and **(L)** relative transcript expression for *Mmp14* in P84 femoral bone preparations. Data are presented with individual samples in

scatterplots and bars corresponding to the mean and standard error of the mean (SEM). Sample sizes, n = 6–8. Scale bars equal 15 μm in all images.

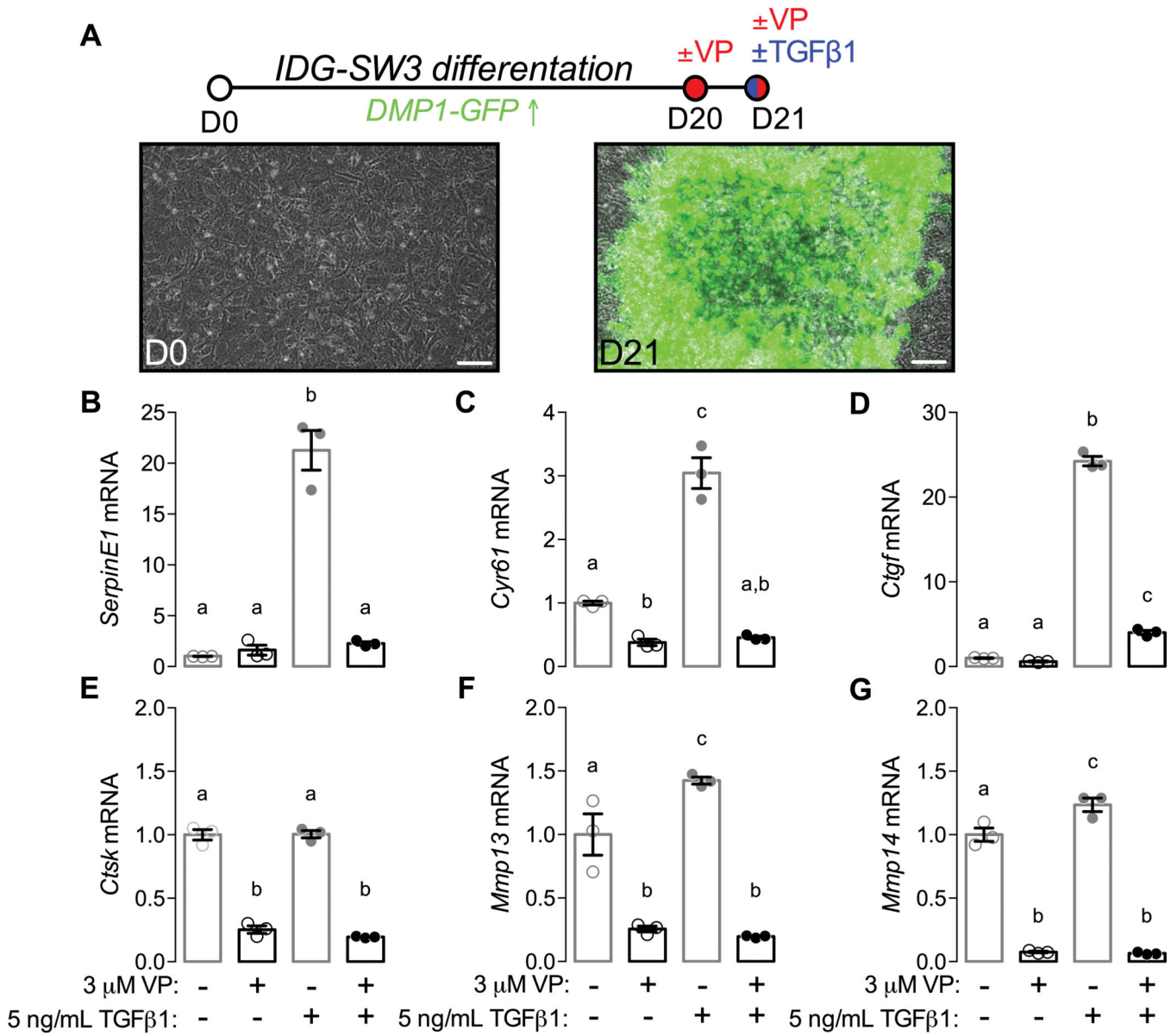

Figure 8. Inhibition of YAP/TAZ-TEAD with verteporfin (VP) reduced TGF-β-induced PLR gene expression *in vitro*.

A) Osteocyte-like IDG-SW3 cells were differentiated for 21 days, with osteocyte differentiation reported by DMP1-GFP transgene expression. Cells were combinatorially treated with inhibitor verteporfin (VP) and/or 5 ng/ml TGFβ1 at day 21. **B-G)** mRNA expression, normalized to *18S rRNA*, was evaluated for **(B)** serpin family E member 1 (*SerpinE1*), **(C)** cysteine-rich angiogenic inducer 61 (*Cyr61*), **(D)** connective tissue growth factor (*Ctgf*), **(E)** cathepsin K **(***Ctsk*), **(F)** matrix metalloproteinase-13 (*Mmp13*), and **(G)** matrix metalloproteinase-14 (*Mmp14*). Relative expression was expressed as fold vs. vehicle (PBS + DMSO)-treated cells. Data are presented with individual samples in scatterplots and bars corresponding to the mean and standard error of the mean (SEM). Sample sizes, N = 3. Scale bars equal 75 mm.

Table 1:

Experimental genotypes & abbreviations.

Genotype	Abbreviation
$Yap^{fl/fl};Taz^{fl/fl}$	$YAP^{WT};TAZ^{WT}$
$Yap^{fl/+};Taz^{fl/+};DMP1^{cre/+}$	$YAP^{cHET};TAZ^{cHET}$
$Yap^{fl/fl};Taz^{fl/+};DMP1^{cre/+}$	$YAP^{cKO};TAZ^{cHET}$
$Yap^{fl/+};Taz^{fl/fl};DMP1^{cre/+}$	$YAP^{cHET};TAZ^{cKO}$
$Yap^{fl/fl};Taz^{fl/fl};DMP1^{cre/+}$	$YAP^{cKO};TAZ^{cKO}$